METAL NANO-PARTICLES AS INCLUSION IN MULTILAYER THINFILM ANTI-REFLECTION COATING TO PROVIDE ULTRAVIOLET BLOCKING

METAL NANO-PARTICLES AS INCLUSION IN MULTILAYER THINFILM ANTI-REFLECTION COATING TO PROVIDE ULTRAVIOLET BLOCKING

A Thesis Presented to

This dissertation has been approved

for the School of Technology by

_____

Faculty of Electrical Engineering Department

Thammasat University

_____

Dean of the School of Engineering

Bangkok University

Deka Sunil, Doctor of Engineering in Electrical and Computer Engineering,

November 2020, School of Technology, Bangkok University

Nano-particles as inclusion in multilayer Thinfilm Anti-reflection Coating to provide Ultraviolet Blocking

Advisor of thesis: Waleed Mohammed, Ph.D.

ABSTRACT

This Thesis is dedicated to proposes the use of Silver metal nanoparticles embedded in TiO2 based porous composite material which tend to mitigate the transmission of near-ultraviolet (UV) radiation across a thin film anti-reflection coating (ARC) arrangement. The proposed structure is based on a double layer porous TiO2 thin film of specific thickness having a definite volume fraction to attain antireflection property. With Silver nanoparticles as inclusion in the upper layer of the double layer thinfilm structure the ultraviolet blocking is optimized in the range of 320nm-400nm. Considering the porous film, the dielectric property of the thinfilm coating can be precisely regulated to achieve effective antireflection properties. The calculations indicated that 10 nm Silver nanoparticles with volume-fraction of 0.01 and film thickness,(51nm top layer & 102nm lower layer) gives the best results for blocking of near UV radiation. Decreasing the aspect ratio of the prolate nano-spheriod gives better UV blocking intensity.

Keywords: Anti-reflection coating, Thinfilm technology, Mixing theory, Nano-particles.

Approved: _____

Signature of Advisor

ACKNOWLEDGMENT

The author is deeply grateful to his advisor Dr. Waleed Mohammed for all his guidance and support received from start to the completion of doctoral degree. He has been a constant source of inspiration throughout the process of the work. The author would like to thank his co-advisor Dr Romuald Jolivot for all the support and encouragement guided to conceive and draft the contents of the chapters. A special thanks for scholarship support by Bangkok University. Finally, the author gratefully acknowledges the technical support by Bangkok University Center of Research in Optoelectronics, Communications and Computational Systems (BU-CROCCS).

TABLE OF CONTENTS

TABLE OF CONTENTS (continued)

LIST OF TABLES

Page

LIST OF FIGURES

LIST OF FIGURES (Continued)

LIST OF FIGURES (Continued)

Page

LIST OF FIGURES (Continued)

CHAPTER 1

INTRODUCTION

Thin film has been utilized for antireflection coating to increase transmissibility and to reduce surface reflections and ghost images (*Anti-Reflective Coatings: A Critical, in-Depth Review - Energy & Environmental Science (RSC Publishing)*, n.d.) (*Opticks: Or, a Treatise of the Reflections, Refractions, Inflections and Colours of Light. The Second Edition, with Additions | Isaac NEWTON*, n.d.) (Yang et al., 2019). This however has (Rayleigh, 1879) placed slight prominence on the reflection of light beyond the range of visible spectrum, precisely the Ultraviolet region (Feuillade & MAURY, 2020) (SR et al., 2016) (*Ultraviolet Radiation: DNA Damage, Repair, and Human Disorders | SpringerLink*, n.d.). The continuous exposure to ultraviolet (UV) radiation can be a ocular hazard in both the natural and occupational environment (International Commission on Non-Ionizing Radiation Protection, 2010) (Bisegna et al., 2018) (Rea, 2000). Exposure to high-intensity Ultraviolet (UVC, unable to penetrate earth's atmosphere.), middle or erythemal Ultraviolet (UVB, largely absorbed by the ozone layer) and near Ultraviolet (UVA, appear to be associated to cancer) in industrial settings causes acute ophthalmic effects [10] (Bullough, 2000). Studies (Ham et al., 1976) (*Ultraviolet Eye Damage: The Epidemiological Evidence*, n.d.) (*Blue Light Hazard and Aniridia. | British Journal of Ophthalmology*, n.d.) have demonstrated that the ultraviolet radiation is not the only contributor to the health hazard. Direct exposure to the short wavelengths of the visible spectrum, termed the “blue light hazard,” (Cid et al., 1998) for an extended period of time

can lead to visual and psychological effect on human. Excessive exposure to harmful blue light, however, is due to the increased use of LED based light sources in the present scenario. Filtration in this range of light spectrum will benefit the humans in terms of visual stimulation and physiological health.

There are wide ranges of industrial application where it is desired to have anti-reflective transparent surface that is clear, colorless and rejects ultraviolet (UV) radiation. Ultraviolet radiation not only causes damage to the eyes and works of art but also contributes to undesirable chemical reaction in various industrial platforms. If light in the range of near UV is exposed on certain pigment over an extended period of time fading can occur. Therefore, it is desirable to broaden the UV blocking towards the region of visible light spectrum in the range of around 380 nanometer (nm) without compromising the properties of visible light.

In the recent years, there has been lot of research papers published in reference to multilayer, broad-band and anti-reflection coatings. This paper relates generally to design anti-reflection coating with ultraviolet radiation block property using layers of explicit thin film for the purposes of extending the effective spectral range and metal nanoparticles for near UV blocking. Composite materials are embedded with inclusions made of different materials with their respective permittivities. The composite materials are considered for fabrication of thin films as it is difficult to procure materials with a specific refractive index (n) in nature and hence avail the characteristic of each inclusion under the desired spectral range. On regulating the nanoparticle size, the peak absorption can be shifted to the wavelength of the desired frequency and regulate the bandwidth

which enhances the absorption of the UV radiation. Moreover, the varying shape helps in the regulation of the width of the spectral band wherein the shorter wavelength of blue light region can be partially blocked.

1.1 Rationale and Problem Statement

The design philosophy of the anti-reflection coating is to attain the state of destructive interference by vary the refractive index of layer while regulating the optical thickness. In order to further enhance the transmission of light through a thin film arrangement, multiple layers coating designed is adopted such that reflections from the surfaces undergo maximal destructive interference in each boundary condition. The number of layers in early AR coatings rarely exceeded three as it is favorable to monitor the deposition of quarter-wave layers while fabricating. The major drawback on considering multiple layers of different material is that it is often difficult to uncover material with desired refractive indices. Furthermore, fewer layers in the ARC do not facilitate in broadening the reflection minimum.

The existing literature suggest that the UVA and major part of blue light spectrum is a source to cause retinal damage and cause disruption to circadian health through suppression of the human melatonin hormone. LED is a potential source of so called "Blue Light Hazard" which has been an integral part of display devises and artificial light source. An antireflective thin film coating in the range of visible light spectra with ultraviolet blocking properties will be beneficial in various optical applications.

1.2 Objectives of Study

The literature on antireflection coatings under thinfilm technology is very widespread and dispersed. There has not been much effort made to map out the various methodologies historically. We shall limit ourselves within the ambit of practical designs simulation and envelop contemporary design methods.

The set of principles and conditions while considering the theoretical approach throughout the study shall be material with light absorption property, dispersion property, and normal light incidence on the subject. Another major restraint in the choice of the thin film material is constrained by the fact that materials with specific refractive index are rare in nature. Composite material will be designed using mixing method for the desired permittivity of the material. Metal nanoparticles of specified dimension is considered for the absorption of the light in the range of high energy blue light and UV-A, hence prevent the transmission across the film. With the property of antireflection along the spectrum of visible light, ultra-violet and the high frequency blue light blocking is subjected on a thin film arrangement.

1.3 Scope of Study

There exist a continuous urge in reducing the refection of light in the visible light spectrum from a surface with the advancement in the thin film deposition technique and plasmonic nanoparticles. The reflection reduction along a broader spectrum can be achieved simply by increase the number of layer of different refractive index and thickness.

While reflection can be reduced significantly using multiple coating, the following deficiencies are mentioned regarding the multiple coating :

1. Present coating is unable to lower the residual reflectance to its minimum potential which is required in specific applications;
2. The reflected light is colored from the coated surface whereas uncoated substrates are neutral in color;
3. Do not pertain to the blocking of near Ultra Violet light.

However the second statement does not pose any substantial effect to our application.

In order to achieve the property of antireflection all along the spectrum of visible light, multilayer antireflection coatings are used extensively in industrial scale. Based on the following ground we shall constrict the design of the anti-reflection coating to heterogeneous multilayer antireflection coatings where the number of layers will be restricted to minimal value for the ease of fabrication. Metal nanoparticles are considered as a constituent inclusion in the composite host material for the absorption of light in the near UV range of light spectrum. The absorption is due to the plasmonic effect of the metal nanoparticles which in turn causes the partial blocking along the high frequency blue light.

UV radiation is a mutagen that changes the genetic material of an organism causing increase in the rate of mutations. UV radiation is a common cause of skin cancer, which affects millions people around the world annually. Polymorphisms of the melanocortin 1 receptor (MC1R) gene in the human body, is sensitive to the ultra violet radiation and enhances the risk of cancer. In addition, the accumulation of mutations due

to the exposure of this radiation reduces the cellular repairing capability which will led to aging process and various disease associated with degeneration of the human body. UV energy is divided in light spectrum as UV-A, -B and -C components. However, the ambient sunlight is predominantly UV-A and UV-B as the ozone in the stratosphere largely absorbs the UV-C. About 90% to 95% of UV-A and 5% to 10% of UV-B reaches the earth surface. UV-A can reach deeper into the dermis region of the skin whereas the UV-B is well absorbed by the epidermis region. UV-A causes damage to the DNA structure of the human body by generating reactive oxygen species. Mutation in the cell can be observed with the direct absorption of UV-B by the DNA.

The intensity of the light varies based on the location of the earth. This geographical change will result in the variation in exposure of ambient UV radiation. The intensity of the UV radiation is higher near the equator as the amount of atmosphere it has to travel is less. The ambient ultraviolet radiation in the earth atmosphere is predominant in the equatorial region over the temperate climate. Moreover, it is observed at as the altitude increases and suspended particulate matter in the air decreases the exposure to the ultraviolet radiation increases. People with fair skin tones are more likely to suffer from skin cancer. The number of patients with skin cancer is increasing at an alarming rate over the recent decades. The role of UV radiation is well conformed as an etiologic agent in causing skin cancer. The UV radiation is more hazardous on the children health over prolong exposure. A moderate exposure to UV radiation in the range of UVB (290-315 nm) has an advantage for vitamin D production in the human body.

However this can be achieved to maintain better immune function, bone, and muscle health while still evading extreme sun exposure.

1.4 Research Questions

How to create a thin film multilayer coating for efficient anti-reflection applications using metal nano-particles to provide ultraviolet blocking?

CHAPTER 2

LITERATURE REVIEW

2.1 Related Literature and Previous Studies

In the resent years, optical industry is ungoing an effort to reduce reflection from the subject by using textured surface or patterns on the reflective surface, which is known as antireflective (or antireflection) coating (ARC). The improvement of antireflection properties in the coating began with Rayleigh (Rayleigh, 1879) in 1879, when it was proposed that the reflectivity in the ambiant surrounding can be reduces by placing a material with reflective index value between the ambiant surrounding and the substrate. However, the effect of anti-reflective property over the coatings surface was proposed by Fraunhofer (Fraunhofer, 1888) in 1817 when he detected the reflection reduction form a substrate as a result of etching a surface in an atmosphere of sulphur and nitric acid vapours.

Over the years there has been various methods and strategies developed in order to reduce the reflection including (but not limited to) single layer, double layer or multiple layer ARCs as well as structuring/patterning of the surface. Almost all of this conventional approach are referred to throughout this review is discussed. Conventional methods are constrained by thickness (quarter/half-wavelength) requirements for interferences. This fundamental limitation deteriorate the scope of improvement of their performance as ARCs, particularly as a result of the prerequisite for thinness and broadband application in many advance optoelectronic devices.

Conventional Antireflective Coatings (ARCs) and Ultra-violet blocking

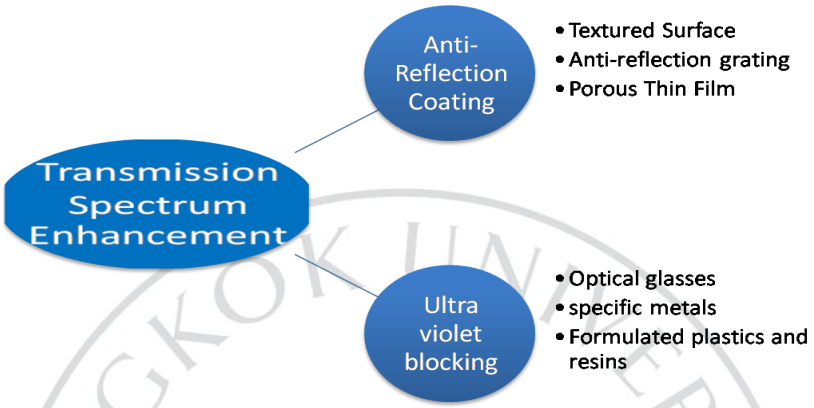

Figure 2.1. Graph representation enhancement of transmission spectra.

Textured Surface

Extensive research has been done in the field of nanotechnology to enhance the antireflection property of a thinfilm. Antireflection coating is effective in reflection if light and reducing glare. Among the various forms of technoogical process to reduce the reflection loss, surface texturization is most prevalent. Surface texturization over the solar cell has contributed to the increase in the light absorption, therfore enhancing the efficiency. Based on the geometrical optics, texturization of the surface is done to increase the interaction of the light within the solar cell by regulating the textured pattern beyond the length of photon wavelength. On varying the thickness and refractive index of ARC'S, we can improve the efficiency of solar cell in terms of short circuit density

Current, $J_{sc} = q \int_{\lambda=0.3\mu m}^{\lambda=1.1\mu m} (1-R(\lambda))N(\lambda)QE(\lambda)d\lambda$, where

$N(\lambda)$ = number of incident photons per cm^2

$QE(\lambda)$ = internal quantum efficiency and

$R(\lambda)$ = textured surface reflectance

Textured surfaces increase the transmission of light into the substrate as compared to the planar surface. Studies have suggested that texturization of a monolayer ARC has the potential to reduce the loss due to reflection by about 2% (*Optical Analysis of Textured Surfaces for Photovoltaic Solar Cells - IEEE Conference Publication*, n.d.). The ray of light with higher angle of incident over the textured Photovoltaic cell holds a significant role in enhancing the reflection (*Characterization and Properties of a Textured Silicon Surface with Nano-Porous Layer - IEEE Conference Publication*, n.d.).

Varous forms of textured surface such as hemisphere arrays and embedded sphere were stuided in the scale of nano-size (Lu & Liu, 2015) where lowest averaged weighted reflectance was observed between the angle of incidence from 0^o to 75^o. The strongest enhancement of localized plasmon effect was observed by the nanoparticles in the range of 60nm. The array of this nanoparticles would result in the enhancement of photon current. An analysis of the light trapping effects of low angle V-grooves shows reduction in the need for an optimum AR coating and high aspect ratio contacts (Jenkins et al., 1992). Nanorod arrays acting as ARCs is also studied for surface reflection and resulting in absorption enhancement into the substarte. It is believed that the nanorod structure can be further optimized to have maximum conversion efficiency of the cell. The enhanced conversion efficiency of surface nanorod-arrays solar cells was investigated where the overall conversion efficiency was enhanced by 10.8% sample (H. W. Wang et al., 2010) .

This increase in the efficiency is contributed from the antireflection and scattering effects of nanorod.

Significant reflection reduction was obtained from the fabricated Si (*Ag-Assisted Electrochemical Etching of Silicon for Antireflection in Large Area Crystalline Thin Film Photovoltaics - IEEE Conference Publication*, n.d.), with about 2% reflection over a wide spectra range (300 to 1050 run) where Random Ag nanostructures were formed on top of the Si surface based on an electro less metal-assisted chemical etching (MacEtch) process (X. Li, 2012). A precise control of etching depth is essential for the reflection reduction in ultra-thin Si films which can be controlled by etching time period.

Antireflection Grating (ARG)

The grating structures work on the same principle of creating a continuous gradient of refrective index. Broadband antireflection requirement over a large spectral range gets fulfilled by the surface relief gratings or ARGs. It is found that the spherical texture grating reduces the reflectivity of the cells in the wavelength regime of 400–1200 nm,thus improves the transmissivity at various incident angles from surface normal to at least 60°.

The antireflection grating property is observed in wide ranges of application staring from solar cell efficiency (Y. Wang et al., 2009), microwave (Mittleman, 2005) and THz (Karlsson & Nikolajeff, 2003) wavelength ranges. Gratings basically help propagate the zeroth diffraction orders (directly transmitted and reflected light) and do not cater to higher diffraction orders which apparently contribute to the total energy

collected in a solar cell. Hence, ARGs have been found to be less effective in case of solar cells. Computational results from a study by Bruckner et al. (Brückner et al., 2007) show that a one dimensional ARG with a triangular cross section and spacing of 50 μm and depth of 100 μm, produces a transmittance of over 99% in the 0.75 to 3 THz range and if the same cross section with revised dimensions, period = 0.5 mm and depth = 1 mm is subjected to the flux, 0.1 - 0.4 THz, shows 99.5% transmission but beyond 0.4 THz, transmission reduces drastically. However, there is a way to avoid the diffraction grating. The period p of the gated structure should follow the relationship $p < \lambda/n_s$ (Gombert et al., 1998).In this scenario, an array of square base pyramids have been reported (Motamedi et al., 1992) to be optimum as the refractive index of the grated system can be approximated to a quintic profile $[n_i + (n_s - n_i) f(\text{thickness}^5)]$ that has already been proved effective in ARCs.

Porous Material

The nano-porous Si layer formation on the top textured surface of mono-crystalline Si contributes to reduction of the reflectance (Bilyalov et al., 2000), thus effecting in improvement of solar cell characteristics. The formation of a porous Si layer about 100nm thick on the textured silicon wafer result in an reflectance lower than 5% in the wavelength region from 500 to 900nm (Lee & Lee, 2006). Porous surface layer might acts as an ARC effecting in the increase of short circuit current and efficiency of solar cell. The technology of porous Si is simple, as well as cheap and it can be adapted

to mass production of solar cells, because simultaneously ARC and surface passivation can be obtained in one electrochemical process (Sarker et al., 2016).

Based on the optical studies using absorption and transmittance measurements show that the roughness at the interface of the porous silicon layer and the silicon substrate is the main cause of the light scattering behavior of the porous silicon structure (Lérondel et al., 1997). The main advantages of the porous silicon layer formation are the simultaneous surface texture and significant reduction of reflection losses.

The luminescent properties of the porous silicon layer may be helpful to convert the high energy UV- and blue part of the spectrum into long wavelength radiations where weakly absorbed long wavelength photons take place uniformly throughout the device regions, such as a solar cell (Vinod & Lal, 2005). Low porosity PS layers have attracted many applications in thin crystalline silicon solar cells for the epitaxial growth and subsequent detachment of the epitaxial layer (*Porous Silicon in Crystalline Silicon Solar Cells: A Review and the Effect on the Internal Quantum Efficiency - Stalmans - 1998 - Progress in Photovoltaics: Research and Applications - Wiley Online Library*, n.d.).

There has been study in the development of the porous silicon based multifunctional materials for the Solar cell based ARC possessing optimal antireflective properties. Porous silicon layers developed by electrochemical and chemical methods allow simplifying the technological cycle, hence reduce the product cost and improve operating characteristics (*Improved Porous Silicon-Based Multifunctional Materials for the Solar Cells Antireflection Coating - IEEE Conference Publication*, n.d.) (Yerokhov & Melnyk, 1999). Plasma etching by $SF_6/0_2$ reactive ion etching is an interesting alternative for the

mask-less texturing of multicrystalline silicon solar cells which helps in homogenous black surfaces with low reflectance and light trapping capacity (Schnell et al., 2000).

Specific Metal-oxide :

Typical optical glasses absorb UV-B radiation to some extent (Taylor, 1989) but insignificant when it comes to UV-A rays, however the absorption increases only gradually considering thin film metallic glasses (TFMGs). Certain metal oxides such as ZnO, CeO2 and TiO2 can be incorporated into glass formulations to impart UV blocking properties. Some oxides may be accommodated, but only in certain proportions (Zhao et al., 2010) (R. H. Wang et al., 2005), and/or in the presence of other components which may be undesirable for the purpose for which the glass is to be used such as coloring of the glass and toxicity (Y. Zhang et al., 2018) (Giovanetti, 2015).

Materials suitable for minimizing UV-A(near UV) results in the partial absorption of visible radiation. This causes coloring of the glass as a result of the presence of impurities in the oxides and/or effect on the glass structure (Karmakar, 2017). This color may be neutralized by the addition of other components but at a loss of visible light transmission. Certain metal oxides can be incorporated into glass formulations to impart UV blocking properties (Zheng et al., 2016) such as titanium dioxide. Titanium dioxide is a strong absorber of UV radiation (Veronovski et al., 2014). Significant absorption begins at a wavelength of about 450 nm (H. Zhang & Zhu, 2012). However, the increase in absorption with decreasing wavelength is very gradual.

The extinction coefficient, k of the thin film TiO2 structure, is 0.0006 (Gottwald et al., 2019)[34] at the wavelength of 400nm. This is equivalent to an absorption coefficient(α) of 1.88×10^4 m^{-1}, using the formula, $\alpha = \frac{4\pi k}{\lambda}$. For 99% of absorption the absorbance(A) of the TiO2 thin film should be around '2'. According to Beer-Lambert law, $I = I_0 e^{-\alpha d}$. Considering log on both sides, we get

$\log_{10}(I_0 / I) = \alpha \times d \times \log_{10}(e)$, where, $\log_{10}(I_0 / I)$ = A. Hence, based on the relation between the thickness(d) of the film and the absorption coefficient, $d = \frac{2.303A}{\alpha}$, the film would need to be in the order of 245μm thick to absorb 99% of the light at 400nm wavelength. Similarly, the thickness of the film should be 822.5nm under the wavelength of 340nm for 99% of absorption. The thickness is still significantly large considering the range of wavelength near the blue light region. Moreover the range of thickness varies to a large extend within the small spectrum of light (340nm- 400nm). The presence of silver nanoparticles of specific size (10nm) will compensate the thickness of the TiO2 thin film within the range of 100nm. Therefore Silver nano-particles are considered within the TiO2 thin film for the absorption of UV radiation in the range of 380nm to 420nm.

Formulated Plastics and Resins :

Specially-formulated plastics and resins are being used for building UV blocking materials. The most common plastic sheet formulations that can filter UV light are UF4 and UF3. UF4 blocks shorter wavelength whereas UF3 blocks longer wavelength

imparting a slight yellow tint (Austin, 1992).Both plastics and resins have a basic drawback, as they are relatively soft and thus will deteriorate under repeated cleaning and external exposure. This substances experience swelling process under humid conditions. Therefore, they must be protected by placing them in assemblies of laminated overcoatings. These measures add significantly to the cost of the finished product.

UnConventional ARCs :

Absorbing ARCs

Attenuation of the light passing through the absorbing film contributes to the reduction (Kumari et al., 2016) (Rensberg et al., 2016) (Berreman, 1963) of reflectance through the surface of a meterial. Oyama and co-workers were the first to used a glass/TiNxOy/SiNx/SiO2 multilayer wherein TiNxOy is an absorber for glass, leading to the concept of an absorbing layer into the ARC community. They were able to optimize the reflection reduction down to 0.1 while the transmission is above 70% (Oyama et al., 1999). Similarly, Ge thin film deposition on the gold mirror results in reflection reduction down to 20% at certain wavelengths due to the strong attenuation of the light at the resonance condition. Whereas reflection can increase upto 80% at certain wavelength (Kats et al., 2013). The loss of the coating should be high enough to compensate for the phase accumulation when the light passes through ultrathin film. Taliercio et al. also observed the strong reflection dip in the system of highly doped InAsSb layers lattice-matched onto GaSb substrates which they also attributed to excitation of the Brewster mode (Taliercio et al., 2014). Similarly, Schlich et al. deposited thin film of silicon on

silicon wafer demonstrated that there exist strong reflection dip at various wavelengths (Schlich & Spolenak, 2013).

Kats et al. also observed change in reflectivity to a large extend in the system of heated film above the transition temperature (Kats et al., 2012). Reflection manipulation by temperature tuning is possible by using phase-changeable VO2 thin film on sapphire substrate for creation of a tunable reflector (absorber). Thin silicon film deposited on an aluminum mirror was fabricated by Mirshafieyan and Guo showing a strong reflection drop depending on the thickness of the coating.

Even though absorbing ARCs is a new area of reasearch in the field of photonics, this class of thin film is not appropriate to many optical application because of the large attenuation and loss.

Plasmonic ARCs :

In order to utilize the plasmonic properties for ARCs application, metallic nanoparticles or nanostructures were fabricated as a coating over the substrate in order to couple the light to the waveguide mode of the substrate or scatter preferentially the light toward the substrate. In principle, because of by the plasmonic nanostructures causes the forward scattering of the incident light (Derkacs et al., 2006) (Nakayama et al., 2008) (Nishioka et al., 2009) (K. X. Wang et al., 2014) and/or electromagnetic confinement around the surface particles (Pillai et al., 2007) (Kim et al., 2008) (Pala et al., 2009), the reflectivity is significantly reduced while providing nearly perfect impedance matching of light to the substrate (Spinelli et al., 2011). This intrinsic loss restricts the applicability of

the plasmonic solar cells to devices wherein the localization and confinement of the light is an advantage, including thermal photovoltaics, thermal collectors and absorbers. In other words, the reflection reduction occurs at the expense of the partial parasitic ohmic loss in the metal (analogous to absorbing ARCs), and can therefore not be used in some optic devices (e.g., glasses, telescopes, lenses, etc.).

2.2 Related Theories

Effective Medium Theory:

In the recent years, much attention has been paid in order to engineer the electrical and optical properties of a composite materials. This composite materials are based on the anisotropic dielectric substrates with metal nanoparticles embedded within it to regulate the overall permittivity and generate plasmonic properties. Based on the permittivity averaging theories, specific effective refractive index can be derived for the desired applications. There exist a number of effective medium theories when engaged on the computational electromagnetics generates the properties of composites material.

Due to the linearity properties of Maxwell Garnett theory it is simple and convenient to model.

A highly improved formulation of effective medium approximation was developed by Maxwell Garnett in the year 1904 (Markel, 2016a). Its aim is to approximate a complex electromagnetic medium such as small particles in a host medium forming a homogeneous effective medium. The Maxwell Garnett mixing formula gives

the permittivity of this effective medium (or, the effective permittivity) in terms of the permittivities and volume fractions of the individual constituents of the complex medium.

A closely related development is the Lorentz molecular theory of polarization. This theory considers a seemingly different physical system: a collection of point-like polarizable atoms or molecules in vacuum. The goal is, however, the same: compute the macroscopic dielectric permittivity of the medium made up by this collection of molecules. A key theoretical ingredient of the Lorentz theory is the so-called local field correction, and this ingredient is also used in the Maxwell Garnett theory.

However, on deriving the Maxwell Garnett theory using the Lorentz local field correction theory it is required to obtain the polarizability. Using this polarizability equation one can obtain the range of validity of the Rayliegh Theory(Cross, 2013). However, MG himself was clear that his relation would only apply correctly for Rayleigh scattering systems when there are "many spheres to a wavelength of light in the medium" (Garnett, 1904). Therefore, we can draw ourselves within the limit of Maxwell Garnett by regulating the validity of Rayliegh Theory of scattering.

Lorentz local field correction formula:

Let us consider some spatial region $\mathbb{R}$ (simple like plane-parallel or a sphere) of volume V containing N>>1 small particles of polarizability α each. The specific volume per one particle is v=V/N. The macroscopic electric field inside the medium is constant, which is important for the argument presented below. Let us now place the whole system

in a constant external electric field E_{ext}. In this case, each dipole is affected by the external field, and therefore it acquires the dipole moment .The total dipole moment is

$$d_{tot} = Nd = N\alpha E_{ext} \tag{2.1}$$

On the other hand, if we assign the sample some macroscopic permittivity ε and polarization $P = \frac{\varepsilon - 1}{4\pi} E$, then the total dipole moment is given by (refer Appendix-I)

$$d_{tot} = VP = V \frac{\varepsilon - 1}{4\pi} E \tag{2.2}$$

In the above expression, E is the macroscopic field inside the medium, which is, of course, different from the applied field E_{ext} .In order to obtain the relation between the two fields; we can use the superposition principle(Bohren, 1986) and write

$$E = E_{ext} + \left\langle \sum_n E_n(r) \right\rangle, \; r \in \mathbb{R} \tag{2.3}$$

Here $E_n(r)$ is the field produced by the nth dipole. Of course the individual fields $E_n(r)$ will fluctuate and so will the sum of all these contribution. We now compute the average as follows:

$$\left\langle E_n(r) \right\rangle = \frac{1}{V} \int_{\mathbb{R}} E_d(r - r_n) d^3 r \approx -\frac{4\pi}{3} \frac{d}{V} \tag{2.4}$$

Where r_n is the location of the nth dipole and $E_d(r) = \frac{3\hat{r}(\hat{r}.d) - d}{r^3}$. In performing the integration, we have disregarded the regular part of the dipole field.

We now substitute equation (2.4) in equation (2.3) and obtain the following result:

$$E = E_{ext} + \sum_n \langle E_n \rangle = E_{ext} - N\frac{4\pi}{3}\frac{d}{V} = \left(1 - \frac{4\pi}{3}\frac{\alpha}{\upsilon}\right)E_{ext} \tag{2.5}$$

In the above chain of equalities, we have used $V / N = \upsilon$ and $d = \alpha E_{ext}$

Substituting the value of E from equation (2.5) in equation (2.2), we get

$$d_{tot} = V\frac{\varepsilon - 1}{4\pi}\left(1 - \frac{4\pi}{3}\frac{\alpha}{\upsilon}\right)E_{ext} \tag{2.6}$$

On substitution of the equation (2.1) in equation (2.6), we get

$$N\alpha E_{ext} = V\frac{\varepsilon - 1}{4\pi}\left(1 - \frac{4\pi}{3}\frac{\alpha}{\upsilon}\right)E_{ext} \tag{2.7}$$

$$\frac{\alpha}{\upsilon} = \frac{\varepsilon - 1}{4\pi}\left(1 - \frac{4\pi}{3}\frac{\alpha}{\upsilon}\right) \tag{2.8}$$

$$\varepsilon = 1 + 4\pi\left(\frac{\alpha}{\upsilon}\right)\left(\frac{1}{1 - \frac{4\pi}{3}\frac{\alpha}{\upsilon}}\right) = \frac{1 + \frac{8\pi}{3}\frac{\alpha}{\upsilon}}{1 - \frac{4\pi}{3}\frac{\alpha}{\upsilon}} \tag{2.9}$$

This is the Lorentz formula for the permittivity of a nonpolar molecular gas. The denominator in Eq. (2.9) accounts for the famous local field correction. The external field E_{ext} is frequently called the local field and denoted by E_L.

Maxwell Garnett Mixing Formula:

Maxwell Garnett attempted to explain the linear optical properties of metal-doped glasses. His model assumed that the inclusion particles were spherical and uniform in size. Under the assumption that the inclusion radius was much smaller than the typical spacing between inclusions, which in turn was much smaller than an optical wavelength, an effective dielectric constant could be determined for the composite. Observing that a metal sphere in the presence of an oscillating electric field emits radiation as if it were an electric dipole, Maxwell Garnett replaced the spheres in the model by the equivalent point dipoles, i.e., he ignored their finite size.

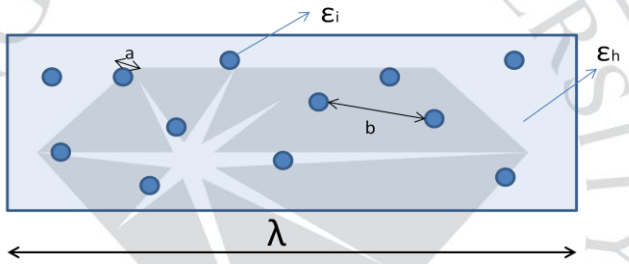

Figure 2.2. Schematic graph of Maxwell Garnett model

We are now ready to derive the Maxwell Garnett mixing formula. We will start with the simple case of small spherical particles in vacuum. Consider spherical particles of radius "a" and permittivity "ε" that are distributed in vacuum either ion a lattice or randomly but uniformly on the average. The volume fraction of the particle is $f = \frac{4\pi}{3}\frac{a^3}{\upsilon}$.

Now on substituting the value of polarizability $\alpha = a^3 \frac{\varepsilon - 1}{\varepsilon + 2}$ and the volume fraction in equation (2.9), we get,

$$\varepsilon_{MG} = \frac{1+\left(\frac{8\pi}{3}\right)\left(a^3\left(\frac{\varepsilon-1}{\varepsilon+2}\right)/\upsilon\right)}{1-\left(\frac{4\pi}{3}\right)\left(a^3\left(\frac{\varepsilon-1}{\varepsilon+2}\right)/\upsilon\right)}$$

$$\varepsilon_{MG} = \frac{1+2f\frac{\varepsilon-1}{\varepsilon+2}}{1-f\frac{\varepsilon-1}{\varepsilon+2}} \qquad (2.10)$$

This is Maxwell Garnett mixing formula for small inclusions in vacuum. But, to have a better understanding about the limitation of Maxwell Garnett we have to observe the static polarizability which has been substituted in the Lorentz local field correction formula in order to attain Maxwell Garnett formula.

Where $\varepsilon = \frac{\varepsilon_i}{\varepsilon_h}$ and $\beta = \frac{\varepsilon_i - \varepsilon_h}{\varepsilon_i + 2\varepsilon_h}$

This above expression displays an important feature: for metal inclusion particles, which have a negative real part of the dielectric constant, the real part of the denominator of β may go to zero, implying the existence of a resonance. Maxwell Garnett compared this resonance with the observed colors of several metal-doped glasses.

Static Polarizability of Dielectrics :

Let us consider a dielectric that is sphere of radius a with dielectric constant ε placed in a uniform electric field, which at large distance from the sphere is directed along the z axis and has magnitude E_0.

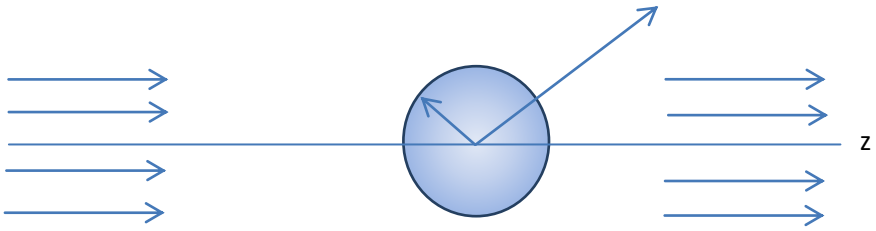

Figure 2.3. Application of external electric field E_0 over a spherical matter of dielectric constant ε

There exist no free charges inside and outside the sphere. The electric field inside and outside the sphere,E_1 and E_2, respectively are derivable from scalar potential $\Phi_{in}(r,\theta)$ and $\Phi_{out}(r,\theta)$. Consequently the problem is of solving the Laplace equation with the proper boundary condition at r=a. From the axial symmetry of the geometry we can take the solution to be of the form a Legendre polynomial expansion. The solution is different for the region inside and outside the sphere and take the form (*Physics 435 -- Prof. S. Errede's Lecture Notes - Fall Semester, 2007*, n.d.) :

$$\Phi_{in}(r,\theta)=\sum_{l=0}^{\infty}A_l r^l P_l(\cos\theta), r<a$$
$$\Phi_{out}(r,\theta)=\sum_{l=0}^{\infty}(B_l r^l + C_l r^{-l-1})P_l(\cos\theta), r>a \quad (2.11)$$

A_l , B_l and C_l are the coefficient which can be determined from the boundary condition. At infinity the boundary condition would led to the relation,

$$\Phi \to -E_0 r\cos\theta, r>>a \quad (2.12)$$

We find that the only non-vanishing B_l is $B_1 = -E_0$. The other coefficient are determined from the boundary condition at r=a. As the electrostatics potential is continuous on the surface it would result in,

$$\Phi_{in}\Big|_{r=a} = \Phi_{out}\Big|_{r=a} \tag{2.13}$$

The normal component of the electric displacement will be continuous on the surface as there are no free surface charge, this would led to,

$$-\varepsilon \frac{\delta\Phi_{in}}{\delta r}\Big|_{r=a} = -\varepsilon_0 \frac{\delta\Phi_{out}}{\delta r}\Big|_{r=a} \tag{2.14}$$

On substituting the series relation(2.9) in the above two boundary conditions we get the following relation.

For the first boundary condition:

$$\sum_{l=0}^{\infty} A_l r^l P_l(\cos\theta) = \sum_{l=0}^{\infty} (-E_O a^l \delta_{1l} + C_l \frac{1}{a^{l+1}}) P_l(\cos\theta) \tag{2.15}$$

Since this equation must be valid for all θ, the coefficient of each Legendre function must be equal and therefore

$$A_l = -E_0 + \frac{C_L}{a^3}$$
$$A_l = \frac{C_L}{a^{2l+1}}, l \neq 1 \tag{2.16}$$

For the second boundary condition:

$$\varepsilon \sum_{l=0}^{\infty} l A_l a^{l-1} P_l(\cos\theta) = \varepsilon_0 \sum_{l=0}^{\infty} \left(-E_0 \delta_{1l} - (l+1) C_l \frac{1}{a^{l+2}} \right) P_l(\cos\theta) \tag{2.17}$$

Since this equation must be valid for all θ, the coefficient of each Legendre function must be equal and therefore

$$\frac{\varepsilon}{\varepsilon_0} A_l = -E_0 - \frac{2C_1}{a^3}$$
$$\frac{\varepsilon}{\varepsilon_0} lA_l = -(l+1)\frac{C_1}{a^{2l+1}}, l \neq 1 \qquad (2.18)$$

The second equation in (2.16) and (2.18) can be satisfied simultaneously only with $A_l = C_l = 0$ for all $l \neq 1$. The remaining coefficients are given in terms of the applied electric field E_0.

$$A_l = -\frac{3}{\varepsilon_r + 2} E_0$$
$$C_l = \frac{\varepsilon_r - 1}{\varepsilon_r + 2} a^3 E_0 \qquad (2.19)$$

The potential is therefore

$$\Phi_{in}(r,\theta) = -\frac{3}{\varepsilon_r + 2} E_0 r\cos\theta, r < a$$
$$\Phi_{out}(r,\theta) = -E_0 r\cos\theta + \frac{\varepsilon_r - 1}{\varepsilon_r + 2} E_0 \frac{a^3}{r^2}\cos\theta, r < a \qquad (2.20)$$

Outside the sphere the potential is equivalent to the applied field E_0 including the field of an electric dipole at the origin with dipole moment

$$P = 4\pi\varepsilon_0 \frac{\varepsilon_r - 1}{\varepsilon_r + 2} a^3 E_0 \quad , \qquad (2.21)$$

oriented in the direction of the applied field. Thus, the applied field induces a dipole moment proportional to the field. The ease with which the sphere is polarize may be specified by polarizability α defined by $P = \varepsilon_0 \alpha E_0$

So finally,

$$\alpha = 4\pi a^3 \frac{\varepsilon_r - 1}{\varepsilon_r + 2} \tag{2.22}$$

The value of $E_d(r)$ from the equation 2.4 is obtained from the relation of polarizability as stated in the above equation 2.22.

Until now our analysis has been restricted to the response of a sphere to an applied uniform static electric field. But we are interested in scattering problem where the applied field is a plane wave that varies in space and time. At any instant the amplitude of the wave illuminating the sphere is $E_0\exp(ikz)$; therefore, if $x=ka<<1$, $E_0\exp(-ika)\approx E_0\exp(-ika)\approx 1$,and the field to which the sphere is exposed is approximately uniform over the region occupied by the sphere.

Again, from equation 2.20 the field inside the sphere is uniform in the electrostatic case. However the field is not expected to be uniform inside the sphere when the external field is a plane wave unless $2\pi k_I a / \lambda << 1$, where k_I is the imaginary part of the particles refractive index. The field changes over a characteristic time of order $\tau = 1/w$, where w is the angular frequency of the incident field. The time τ^* required for a signal to propagate across the sphere is of order an_I / c , where n_I is the real part of the particles refractive index and c is the speed of light in vacuum. Thus, when the incident

light changes, every point of the sphere will get the message provided that $\tau^* \ll \tau$ or, equivalently, $2\pi na/\lambda << 1$. The two inequalities involve the real and the imaginary part of the refractive index may be combined into a single inequality: $|m|x << 1$

Influence of material property on absorption efficiency :

The absorption and scattering efficiencies of a small sphere may be written as

$Q_{abs} = 4x\,\mathrm{Im}\dfrac{\varepsilon-1}{\varepsilon+2}$ and $Q_{sca} = \dfrac{8}{3}x^4\left|\dfrac{\varepsilon-1}{\varepsilon+2}\right|^2$, where the quantity $\dfrac{(\varepsilon-1)}{(\varepsilon+2)}$ appears in the problem of a sphere embedded in a uniform static electric field (Bohren & Huffman, 2008)[20]. This suggests a connection between electrostatics and scattering by particles small as compared to the wavelength. Hence, there is an indirect relation between the scattering of light phenomenon and the Maxwell Garnett mixing theory.

Let us try to understand the relation between the two similar identities in different equations :

The extinction and scattering efficiencies are (to terms of order x^4)

$$Q_{abs} = 4x\,\mathrm{Im}\left\{\frac{\varepsilon-1}{\varepsilon+2}\left[1+\frac{x^2}{15}\left(\frac{\varepsilon-1}{\varepsilon+2}\right)\frac{\varepsilon^2+27\varepsilon+38}{2\varepsilon+3}\right]\right\}+\frac{8}{3}x^4\,\mathrm{Re}\left\{\left(\frac{\varepsilon-1}{\varepsilon+2}\right)^2\right\},$$

$$Q_{sca} = \frac{8}{3}x^4\left|\frac{\varepsilon-1}{\varepsilon+2}\right|^2 \qquad (2.23)$$

Where, $m = \dfrac{k_I}{k} = \dfrac{N_I}{N}$, $x = ka = \dfrac{2\pi Na}{\lambda}$, $m = \dfrac{k_I}{k} = \dfrac{N_I}{N}$

N_I and N are the refractive indices of particles and medium, respectively.

If $|\varepsilon| x << 1$, the coefficient of $\frac{\varepsilon - 1}{\varepsilon + 2}$ in the first term of equation (2.23) is approximately unity; with this restriction, the absorption efficiency is

$$Q_{abs} = 4x \operatorname{Im}\left\{\frac{\varepsilon - 1}{\varepsilon + 2}\right\}\left[1 + \frac{4}{3}x^3 \operatorname{Im}\left\{\left(\frac{\varepsilon - 1}{\varepsilon + 2}\right)\right\}\right] \tag{2.24}$$

Therefore, if $\frac{4}{3}x^3 \operatorname{Im}\left\{\left(\frac{\varepsilon - 1}{\varepsilon + 2}\right)\right\} << 1$, a condition that will be satisfied for sufficiently small x, the absorption is approximately

$$Q_{abs} = 4x \operatorname{Im}\frac{\varepsilon - 1}{\varepsilon + 2} \tag{2.25}$$

Now, the relation that has been obtain, a part of it can be matched with the Maxwell Garnett formula provided the condition is availed to obtain the equation (2.25). To the extent that this is a good approximation(Heller, 1965), the absorption cross-section $C_{abs} = \pi a^2 Q_{abs}$ is proportional to the volume of the particles.

The interaction between the reflected and refracted light from multiple layers leads to ghost image where fake image or blurred image of a subject or light source is observed respectively. Ghost image should not be formed near the focal plane as it produces a disturbing effect over the actual image and there should not have high intensity light source along the primary source and object.

2.3 Hypothesis

In the range of visible light spectrum, the suggested arrangement of thin films design act as an antireflection coating which have the property of partial blocking both

the UV radiation(in the range of 320nm-370nm) and high frequency blue light radiation. With the metal nanoparticles embedded in the thin film layer it is possible to design antireflection coating with the property of near UV blocking. Regulating the shape and size of the nanoparticles would lead to the shifting of transmission dip within the range of ultra violet radiation.

2.4 Theoretical Framework

The validation of Maxwell Garnett model is limited within the dilute conductive phase of the dielectric composites. Quasistatic approximation is involved in this model. The significant fearures of Maxwell Garnett are mentioned as (Markel, 2016c) below:

1. The resultant composite mixture is isotropic in an electrodynamic environment;
2. The constitutive parameter of the Maxwell garnett is indipendent of the electromagnetic field intensity, hence linearity of the system can be attained;
3. On the exposure of forces such as electrical and mechanical over the composite substance its parameter will not alter with the change in time, hence the substance is non-parametric;
4. In order to retain the validity of the theorem, the inclusion within the host medium should be at a distance seperated well beyond its diameter.
5. The wavelength of the incident light over the composite material is comparable or greater than the characteristic diameter of the inclusion within the host medium;
6. In general spherical shape of the inclusion is considered, however on considering ellipsoilad shape it is randomly oriented within the composite material;

7. The volume fraction of the conducting inclusions within the host material should be less than the percolation threshold of the mixture material.

An effective medium is derived based on the formula of Maxwell Garnett. This effective medium has a new effective permitivity deduced from the individual constituent (its permittivities and volume fractions) of the composite medium. A complex medium is considered where the inclusions are spherical in shape of radius 'a' with permittivity 'ε' are randomly orianted in the vaccum as the host medium uniformly. On considering a specific particle with the overall host volume enclosing it generates specific volume 'v', and the volume fraction of spherical inclusions in the vaccum host medium is $f = (4\pi/3)(a^3/v)$. Based on the Maxwell Garnett theorem, the new effective permittivity of the complex medium is figured as

$$\varepsilon_{MG} = \frac{1+2f\dfrac{\varepsilon-1}{\varepsilon+2}}{1-2f\dfrac{\varepsilon-1}{\varepsilon+2}} \tag{2.26}$$

ε_{MG} is the effective permittivity of composite material based on Maxwell Garnett mixing formula. The effective permittivity (ε_{MG}) of the engineered material can be deviated from the permitivity of naturally found material, contrasting in the Lorentz theory of polarization. The earlier assumption was that the host medium was considered to be vaccum which is not realistic for a composite material. Therefore, a physical medium of specific permittivity is considered as a back ground medium. The new effective medium with host permittivity is stated as

$$\varepsilon_{MG} = \varepsilon_h \frac{1+2f\frac{\varepsilon_i-\varepsilon_h}{\varepsilon_i+2\varepsilon_h}}{1-2f\frac{\varepsilon_i-\varepsilon_h}{\varepsilon_i+2\varepsilon_h}} \quad (2.27)$$

Where

ε_h is the permittivity of the host medium and

ε_i is the permittivity of the inclusions embedded in host medium.

f is the volume fraction of inclusions in the composite material.

In order to normalize the equation 2.27 to more generalized form following substitution is carried out: $\varepsilon_{MG} \rightarrow \varepsilon_{MG}/\varepsilon_h$ and $\varepsilon \rightarrow \varepsilon_i/\varepsilon_h$.

Based on the study from Figure 2.4 and Figure 2.5 we can infer that the real and imaginary part of the complex permittivity of the composite material can be changed with the regulation of the inclusion volume fraction. The change in the permittivity implies the corresponding change in the refractive index of the complex medium. From this, a desired value of volume fraction can be considered to obtain the required complex refractive index. Moreover, with the change in the type of inclusion where gold and silver is considered, an assorted pattern of change is observed in refractive index.

Maxwell Garnett model over Bruggeman theory :

There exist various theory based on effective medium approximation where the applicability is dependent on the volume fraction of the inclusions, the permittivity of the constituent components and inhomogeneity of metal or dielectric nanoparticles as inclusion in terms of its dimension. Maxwell-Garnett theory holds its validation under the condition when the concentration of inclusions is less in the host medium with the

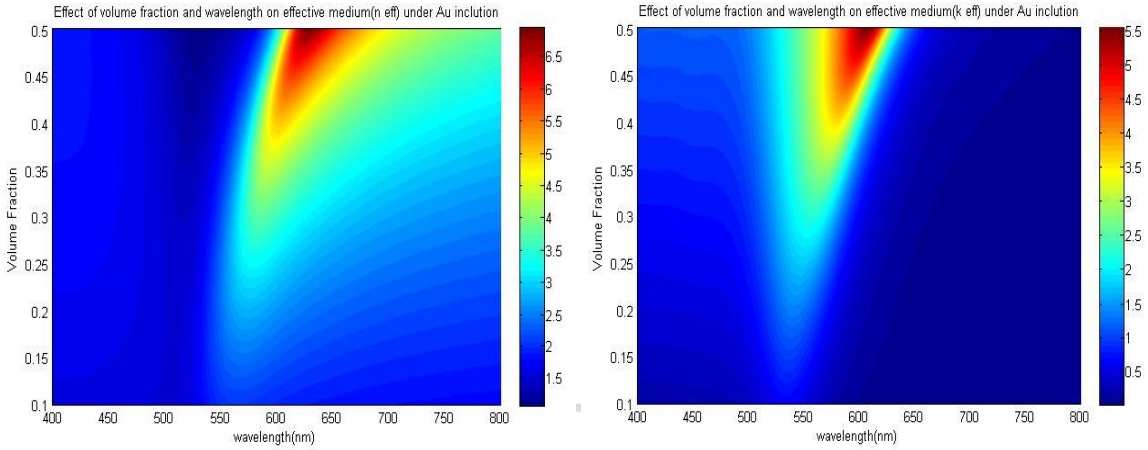

(a) (b)

Figure 2.4. Medium –SiO2 ;Inclusion-Au ; light normal incidence to plain.(a)the effect of volume fraction in the real part of the refractive index.(b) the effect of volume fraction in the imaginary part of the refractive index.

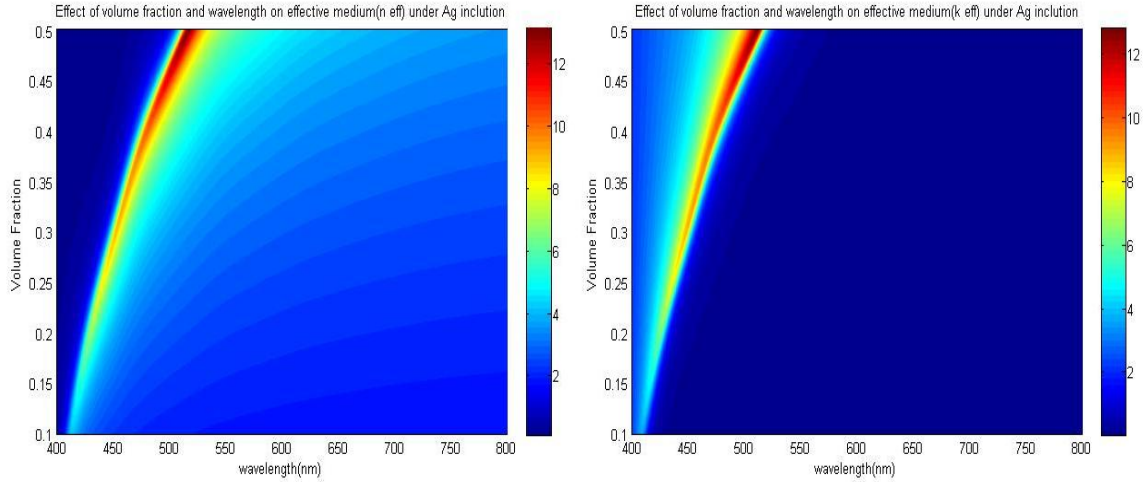

(a) (b)

Figure 2.5. Medium- SiO2; Inclusion-Ag; light normal incidence to plain.(a)the effect of volume fraction in the real part of the refractive index.(b) the effect of volume fraction in the imaginary part of the refractive index.

spherical shape (Koledintseva et al., 2006). When the concentration of the inclusion is comperatively higher within the composite medium, Bruggeman theory is more pertinent to apply.

However this theory involves obscure approach when the nanosize inclusions is drawn towards ellipsoidal shape(Markel, 2016b) and complex roots for algebric equation for the perfect sphere particles in the dielectric host medium. We opt for Maxwell-Garnett from the range of various mixing theory because of its simplicity in computational approach and rapid numerical methodology for permittivity averaging under electromagnetic field.

Nano-particle size effect :

The formulation of Maxwell-Garnett theory is based on the condition where the inclusions are small as compared to the wavelength of the interacting light spectrum. Maxwell-Garnett equation does not take particle size into consideration as its size is assumed to be well below the length of the light wave. As in the case of Mie theory, the size effect can be embraced on extinction maxima. In order to include the shape effect, a screening parameter 'k', is incorporate into the Maxwell-Garnett equation. The numerical value of 'k' as 2 is considered for spherical particles in the general equation of Maxwell-Garnett $\left(\frac{\varepsilon_{MG}-\varepsilon_h}{\varepsilon_{MG}+2\varepsilon_h}\right)=f_m\left(\frac{\varepsilon_i-\varepsilon_h}{\varepsilon_i+2\varepsilon_h}\right)$. Hence, the screening parameter will decide the change of optical properties for the change in inclusion shape and size.

Dynamic Maxwell Garnett approach:

To observe the size effect of nanoparticles inclusion in a composite medium an alternate approach was adopted by Meier and Wokaun for the depolarization factor. As metal nonoparticles are considered, the surface enhance raman scattering (SERS) is observed under the influence of the oscillating electromagnetic radiation.

In general, the shape of the inclusion is spherical with radius 'a'. The effective depolarization factor q_{eff} , is a function of the radius 'a' and permittivity of the host material under a particular wavelength via

$$q_{eff} = \frac{1}{3} - \frac{1}{3}k^2a^2 - \frac{2}{9}ik^3a^3 \tag{2.28}$$

where

i. The first term 'q =1/3' is the Lorentz depolarizing factor (under spherical shape).

ii. The second term indicates the existence of dynamic depolarization (generate different phase of incident light within the particles as the size is comparable to the incident wavelength)

iii. The third term indicates the damping of the induced dipole (the damping is due to the radiation emission from the particles within)

Where $k = 2\pi n_h / \lambda$, n_h is the refractive index of the host medium.

Effective screening factor k_{eff} is related using effective depolarization factor using,

$$k_{eff} = (1/q_{eff}) - 1 \tag{2.29}$$

As the numerical value ‘2’ was considered for spherical size, generalizing for all the shape k_{eff} is considered over ‘2’ in the Maxwell Garnett equation; hence Maxwell Garnett equation leads to

$$\left(\frac{\varepsilon_{MG}-\varepsilon_h}{\varepsilon_{MG}+k_{eff}\varepsilon_h}\right)=f_m\left(\frac{\varepsilon_i-\varepsilon_h}{\varepsilon_i+k_{eff}\varepsilon_h}\right) \tag{2.30}$$

NOTE:

The original Maxwell-Garnett's theory for anisotropic inclusion in the host medium was considered to be spherical. For the spherical geometry the factor ‘2’ appears in the Maxwell-Garnett's equation. The factor where ‘2’ emerges in the equation 2.26 is termed as the screening parameter. The screening parameter is denoted as “k”. If the geometry tends to be spike like particles leaning with their axes of revolution along the direction of incident light, the “k” value will draw towards unity. Whereas, if the geometry tends to be plane disk like particles leaning with their axes of revolution along the direction perpendicular of incident light, the “k” value will approach towards infinity. Now, we obtain an equation for the effective permittivity of the medium as

$$\left(\frac{\varepsilon_{MG}-\varepsilon_h}{\varepsilon_{MG}+k_{eff}\varepsilon_h}\right)=f_m\left(\frac{\varepsilon_i-\varepsilon_h}{\varepsilon_i+k_{eff}\varepsilon_h}\right)$$

$$(\varepsilon_{MG}-\varepsilon_h)(\varepsilon_i+k_{eff}\varepsilon_h)=f_m(\varepsilon_{MG}+k_{eff}\varepsilon_h)(\varepsilon_i-\varepsilon_h)$$

$$\varepsilon_{MG}(\varepsilon_i+k_{eff}\varepsilon_h)-\varepsilon_h(\varepsilon_i+k_{eff}\varepsilon_h)=f_m\varepsilon_{MG}(\varepsilon_i-\varepsilon_h)+f_m k_{eff}\varepsilon_h(\varepsilon_i-\varepsilon_h)$$

$$\varepsilon_{MG}\{(\varepsilon_i+k_{eff}\varepsilon_h)-f_m(\varepsilon_i-\varepsilon_h)\}=f_m k_{eff}\varepsilon_h(\varepsilon_i-\varepsilon_h)+\varepsilon_h(\varepsilon_i+k_{eff}\varepsilon_h)$$

$$\varepsilon_{MG}=\varepsilon_h\frac{f_m k_{eff}(\varepsilon_i-\varepsilon_h)+(\varepsilon_i+k_{eff}\varepsilon_h)}{(\varepsilon_i+k_{eff}\varepsilon_h)-f_m(\varepsilon_i-\varepsilon_h)} \tag{2.31}$$

Limitation of dynamic Maxwell Garnett equation :

In general cases, the Maxwell Garnett approximation overestimated λ_{max} (wavelength of maximum extinction) under dynamic approach. This effect is more prominent when considering nanoparticles with larger radius. The scattering losses of a substrate is included within the absorption coefficient, k_c under the dynamical Maxwell Garnett model. This approach do not accounts for extrinsic size effect and intrinsic confinement. Nevertheless, it offers simplicity to a certain degree and a rational description of λ_{max} in terms of band intensity and band shape.

Contribution of Host Medium over light scattering and other effects:

A localized field enhancement is bound to be observed if electron transfer can be observed amid the inclusion metal nanoparticle and the dielectric host medium. Considering the gold metal nanoparticles, the energy under electromagnetic enhancement is well below 2eV around the wavelength of 620nm and diminishes below this energy. The surface electromagnetic enhancement is predominant at longer wavelength, where Plasmon resonance would be strongest for $\theta=0^0$ polarization, for a template synthesis of Gold nanoparticles. The higher extinction in the dipole resonance is expected to be at the angle of $\theta=0^0$ than $\theta=90^0$ case, while considering the polarization of the Au nanoparticles. Based on the electro dynamic effects of small particles studied by Meier and Wokaun and Zeman and Schatz, the smaller the particles the higher is the surface electromagnetic enhancement. The attenuation of electromagnetic enhancement with the increase in particles size is observed due to radiation damping.

The size variation leads to the following effect:

1. The difference between the scattering matrix calculations and the experimental polarization spectra reduces, as the inclusion nanoparticle radius increases.
2. With the increase in the nanoparticles size the difference of the calculated extinction intensity between the θ= 0° and θ= 90° dipolar resonances is reduced.

There are various parameters that need to be taken into account by rigorous semi-analytical scattering treatment to observe the dependence of θ over the extinction intensities for the particles with larger dimension. On considering smaller inclusions, more complex relationship between metal nanoparticles along with their host medium has to be assumed as nanoparticles would results to higher surface electromagnetic enhancements in a thinfilm.

Light Interference in the Effective Medium :

Based on the poynting vector, the power per unit area crossing a surface under vaccum whose normal is parallel to the S vector, is given by

$$\vec{S} = c^2 \varepsilon_0 \vec{B} \times \vec{E} \tag{2.32}$$

Irradiance (radiant flux density, W/m^2) is $I = \langle S \rangle_T = \frac{c\varepsilon_0}{2} E_0^{\,2}$ (2.33)

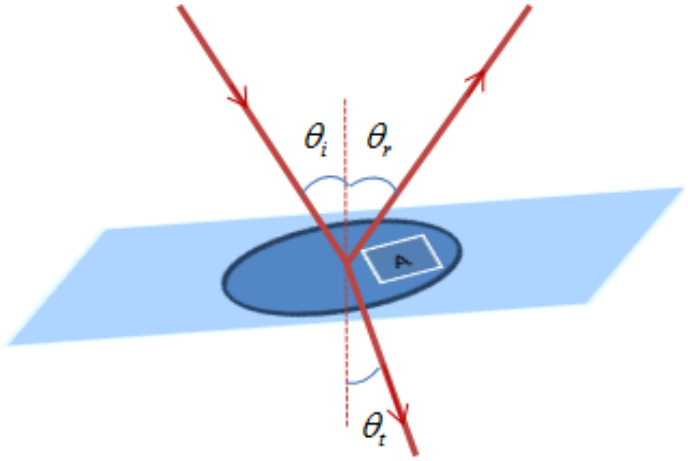

Figure 2.6. Incident light over a plane surface at an angle of incident

Let, I_i is the incident flux densities

I_r is the reflected flux densities

I_t is the transmitted flux densities.

Accordingly, the incident power is $I_i A\cos\theta_i$, reflected power is $I_r A\cos\theta_r$ and transmitted power is $I_t A\cos\theta_t$ through A.

Reflectance R, is given by

$$R = \frac{I_r A\cos\theta_r}{I_i A\cos\theta_i} = \frac{I_r}{I_i} \tag{2.34}$$

Where the numerator is the reflected power and the denominator is the incident power in the RHS of the equation 2.34.

The transmittance T is given by

$$T = \frac{I_t \cos\theta_t}{I_i \cos\theta_i} \tag{2.35}$$

Where the numerator is the transmitted flux and the denominator is the incident flux in the RHS of the equation 2.35.

The quotient $\frac{I_r}{I_i} = \frac{v_r \varepsilon_r E_r^{\,2}/2}{v_i \varepsilon_i E_i^{\,2}/2}$ and since there is no change in the medium for the incident and reflected wave and $R = \frac{E_r^{\,2}}{E_i^{\,2}} = r^2$, the transmittance is

$$T = \frac{n_t \cos\theta_r}{n_i \cos\theta_i}\left(\frac{E_t^{\,2}}{E_i^{\,2}}\right) = \left(\frac{n_t \cos\theta_t}{n_i \cos\theta_i}\right) t^2 \text{ (assuming } \mu_i = \mu_r = \mu_0) \tag{2.36}$$

where we use the relation as $\mu_0 \varepsilon_t = 1/v_t^{\,2}$ and $\mu_0 v_t \varepsilon_t = n_t / c$

The reason for not considering T as t^2 is for the following two reasons:

1) the ratio of indices of refraction must be there, since the speed at which energy is transported into and out of the interface are different.

2) the cross sectional areas of incident beams are not equal to the reflected beams. According to the conservation of energy

$$I_i A\cos\theta_i = I_r A\cos\theta_r + I_t A\cos\theta_t \tag{2.37}$$

$$n_i E_i^{\,2}\cos\theta_i = n_i E_r^{\,2}\cos\theta_i + n_i E_t^{\,2}\cos\theta_t \tag{2.38}$$

$$1 = \frac{E_r^{\,2}}{E_i^{\,2}} + \frac{n_i E_t^{\,2}\cos\theta_t}{n_i E_i^{\,2}\cos\theta_i} \tag{2.39}$$

This is simply, 1=T+R where there is no absorption. We are considering a lossless antireflection coating at the present state hence we will abide by the above rule.

Multiple-beam Interference :

In general a Fabry–Pérot interferometer or etalon is modeled with two reflecting surfaces on a transparent plate. The interference of the reflected and transmitted light is evident to observe the reflectivity and transmissivity of the plate surface which would be considered as the antireflection coating over the substrate material.

The interference between the multiple reflections and transmissions of light between the two parallel reflecting surfaces of etalon cause a varying transmission function. A peak in the amplitude of transmission light through the etalon is observed if the transmitted beams are in phase which is termed as constructive interference. Minimum transmission is observed if the transmission beams are out-of-phase which is termed as destructive interference.

The constructive and destructive interference due to the interaction between the multiple reflected and transmitted beams are dependent on the following factors:

i) the width of the etalon (*h*),

ii) the refractive index of etalon (*n*),

iii) the wavelength (λ_0) of the incident light ray in vacuum,

iv) the angle of transmission(θ) through the etalon .

A phase difference is generated between the successive transmitted light ray as the radiation is subjected to change in medium which is given by

$$\delta = \frac{4\pi}{\lambda_0} nh\cos\theta \tag{2.40}$$

For better assessment of the condition let us consider plane-surface plate having a refractive index n_i . A substrate with refractive medium n_s is layered below the plane-

parallel plate within a medium of refractive index n_c. Let us suppose that the angle of incident is θ_i and angle of transmission is θ_t for a monochromatic light over the plane of incidence.

Based on the figure 3.3, it is observed that there exist two individual plane waves where one lies along the incident plane wave with refractive index n_c and the other is transmitted into the plate refractive index n_i. The transmitted light is incident over the second surface of the plane wave plate at angle θ_t and is further divided into two plane waves. The transmitted part is directed below and the other reflected part is back into the plane above; and the process of multiple division of wave in each boundary layers is indicated in the figure below.

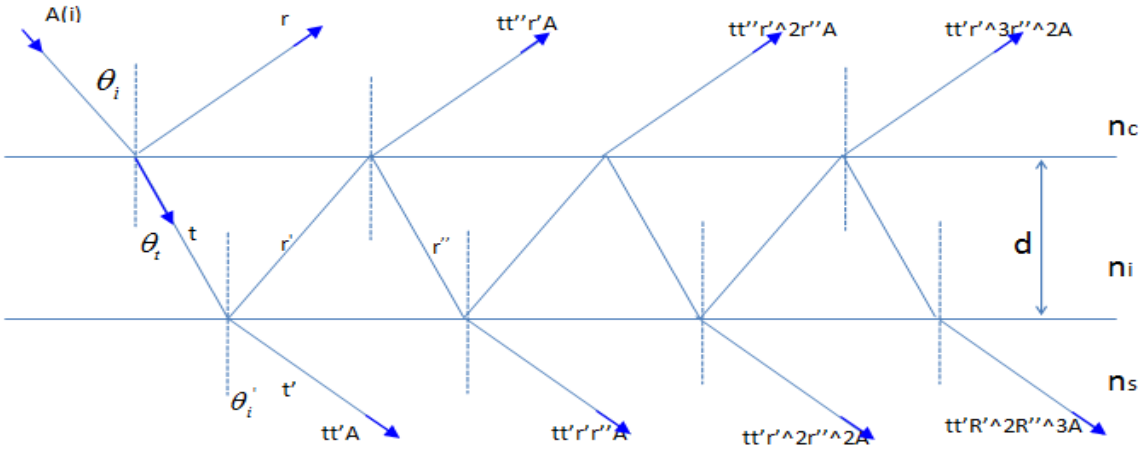

Figure 2.7. Interference between the multiple reflections of light between the two reflecting surfaces

The primary incident i^{th} light wave has amplitude of A^i, which is considered to be polarized linearly. The electric field vector is either parallel or perpendicular to the plane of incidence. Let A^i be the amplitude of the electric vector of the incident wave, which we assume to be linearly polarized, with the electric vector either parallel or perpendicular to the plane of incidence. Consider, 'r' be the reflection coefficient for the ray of primary light first reflected over the plane surface plate. Reflection coefficient is the ratio of reflected light and incident light amplitude. The subsequent rays of light developed due to divisions of light in each boundary condition generates secondary reflection coefficient and incident coefficient such as $r^{'}$, $t^{'}$, $r^{''}$, $t^{''}$……respectively.

On considering the effect of combined reflected rays of light from the surface of the plane parallel plate, the sum of complex amplitude is

$$A^{(r)} = rA^{(i)} + tt^{"}r^{'}A^{(i)}e^{i\delta} + tt^{"}r^{'2}r^{"}A^{(i)}e^{2i\delta} + tt^{"}r^{'3}r^{"2}A^{(i)}e^{3i\delta} + tt^{"}r^{'4}r^{"3}A^{(i)}e^{4i\delta} + ...$$

$$= rA^{(i)} + tt^{"}r^{'}A^{(i)}e^{i\delta}(1 + r^{'}r^{"}e^{i\delta} + r^{'2}r^{"2}e^{2i\delta} + r^{'3}r^{"3}e^{3i\delta} + ...$$

$$= rA^{(i)} + tt^{"}r^{'}A^{(i)}\left(\frac{1}{1-r^{'}r^{"}e^{i\delta}}\right)e^{i\delta}$$

$$R = r + \left(\frac{tt^{"}r^{'}e^{i\delta}}{1-r^{'}r^{"}e^{i\delta}}\right) \qquad (2.41)$$

Where,

$$r = \frac{n_c\cos\theta_i - n_i\cos\theta_t}{n_c\cos\theta_i + n_i\cos\theta_t}; r^{'} = \frac{n_i\cos\theta_t - n_s\cos\theta_i^{'}}{n_i\cos\theta_t + n_s\cos\theta_i^{'}}; r^{"} = \frac{n_i\cos\theta_t - n_c\cos\theta_i}{n_i\cos\theta_t + n_c\cos\theta_i}$$

Similarly, the effect of combined transmitted rays of light from the lower surface of the plane parallel plate, the sum of complex amplitude is

$$A^{(t)} = tt^{'}A + tt^{'}r^{'}r^{"}A^{(i)}e^{i\delta} + tt^{'}r^{'2}r^{"2}A^{(i)}e^{2i\delta} + tt^{'}r^{'3}r^{"3}A^{(i)}e^{3i\delta} + \ldots\ldots\ldots$$
$$= tt^{'}A^{(i)}e^{i\delta}(1 + r^{'}r^{"} + r^{'2}r^{"2} + r^{'3}r^{"3} + \ldots\ldots\ldots$$
$$= tt^{'}A^{(i)}\left(\frac{1}{1 - r^{'}r^{"}e^{i\delta}}\right)$$
$$T = \frac{tt^{'}}{1 - r^{'}r^{"}e^{i\delta}} \qquad (2.42)$$

where,

$$t = \frac{2n_c\cos\theta_i}{n_c\cos\theta_i + n_i\cos\theta_t} \;;\quad t^{'} = \frac{2n_i\cos\theta_t}{n_i\cos\theta_t + n_s\cos\theta_i^{'}} \;;\quad t^{"} = \frac{2n_i\cos\theta_t}{n_i\cos\theta_t + n_c\cos\theta_i}$$

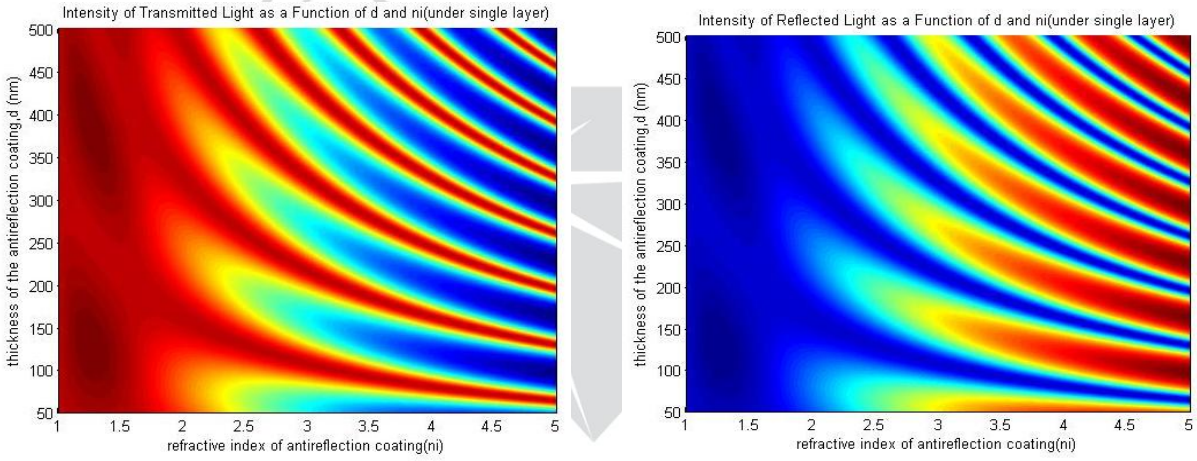

Figure 2.8. Effect of light intensity with the change of AR coating thickness and refractive index. Ns (substrate)=1.6 & light normal to plane under 550 nm wavelength

From the figure 2.8, it is quite distinctive that with the change in the thickness of the antireflection coating of single layer the reflectance and transmittance can be regulated. Here, in the Figure 2.8 it can be observe that with the varying thickness the minimum reflection is observed around refractive index between 1 and 1.5.

Transfer Matrix Method :

Transfer Matrix Method is one of the basic computational electromagnetic approaches to attain the optical response of stratified medium. This approach generates a characteristic matrix which relates the effect of electric and magnetic field at each boundary condition of an optical element. An anti-reflection coating arrangement is considered where the ray of light has to travel through four different layers (first is the ambiance, next two is the double layer antireflection coating and fourth is the silicon substrate) with specific reflective index. The boundary conditions have to be fulfilled at interface.

Double layer condition:

First Boundary Condition

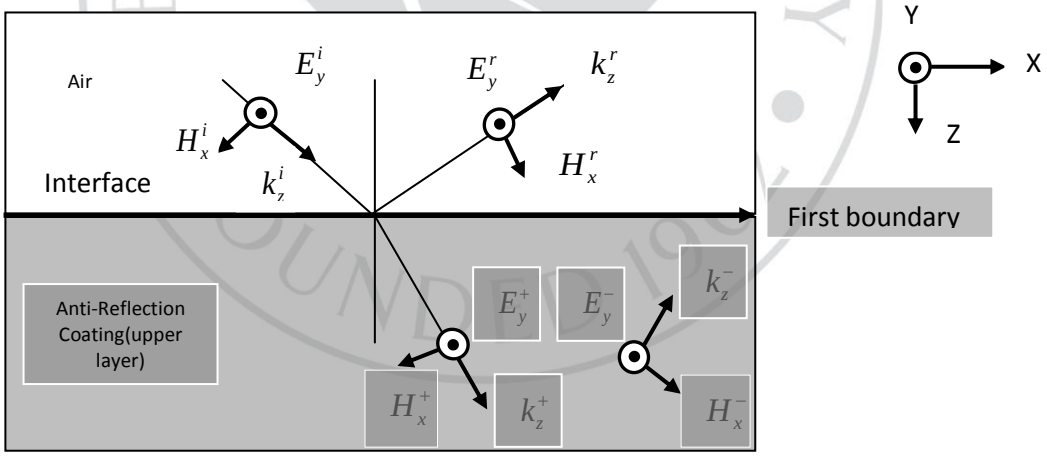

Figure 2.9. First boundary condition between two dielectric media

Under electric field continuity in the first boundary,

$$E_y^i + E_y^r = E_y^+ + E_y^- \tag{2.43}$$

Again, under magnetic field continuity in the first boundary,

$$H_x^i + H_x^r = H_x^+ + H_x^- \tag{2.44}$$

Maxwell's equations under boundary condition can be written as

$$\begin{bmatrix} \hat{x} & \hat{y} & \hat{z} \\ k_x & k_y & k_z \\ E_x & E_y & E_z \end{bmatrix} = w\mu \begin{bmatrix} H_x \\ H_y \\ H_z \end{bmatrix} \tag{2.45}$$

If E is along y and H is in the x-z plane, Maxwell's equations can be written

$$\begin{bmatrix} \hat{x} & \hat{y} & \hat{z} \\ k_x & 0 & k_z \\ 0 & E_y & 0 \end{bmatrix} = w\mu \begin{bmatrix} H_x \\ 0 \\ H_z \end{bmatrix} \tag{2.46}$$

Hence, we observe that $H_x = k_z E_y / w\mu$

Similarly,

$$H_x^i = k_z^i \times E_y^i / \mu w; H_x^r = k_z^r \times E_y^r / \mu w; H_x^+ = k_z^+ \times E_y^+ / \mu w; H_x^- = k_z^- \times E_y^- / \mu w \tag{2.47}$$

Substituting the values of equation (3.47) in (3.46), we get

$$k_z^i E_y^i + k_z^r E_y^r = k_z^+ E_y^+ + k_z^- E_y^- \tag{2.48}$$

As we know that

$$k_z^i = -k_z^r \; ; \; k_z^+ = -k_z^- \quad \& \quad k_z^i \left(E_y^i - E_y^r\right) = k_z^+ \left(E_y^+ - E_y^-\right) \tag{2.49}$$

Using equation (2.43) and (2.49), we get

$$\begin{bmatrix} 1 & 1 \\ k_z^i & -k_z^i \end{bmatrix} \begin{bmatrix} E_y^i \\ E_y^r \end{bmatrix} = \begin{bmatrix} 1 & 1 \\ k_z^+ & -k_z^+ \end{bmatrix} \begin{bmatrix} E_y^+ \\ E_y^- \end{bmatrix} \tag{2.50}$$

Now,

$$k_z^i = \frac{2\pi n_0}{\lambda} \cos\theta_0 \; ; \quad k_z^+ = \frac{2\pi n_1}{\lambda} \cos\theta_1 \; ; \; k_z^{+(2)} = \frac{2\pi n_2}{\lambda} \cos\theta_2 \tag{2.51}$$

Let,

$$A=\begin{bmatrix}1 & 1\\ k_z^i & -k_z^i\end{bmatrix} B=\begin{bmatrix}1 & 1\\ k_z^+ & -k_z^+\end{bmatrix} \tag{2.52}$$

$$\begin{bmatrix}E_y^+\\ E_y^-\end{bmatrix}=AB^{-1}\begin{bmatrix}E_y^i\\ E_y^r\end{bmatrix} \tag{2.53}$$

Second Boundary Condition:

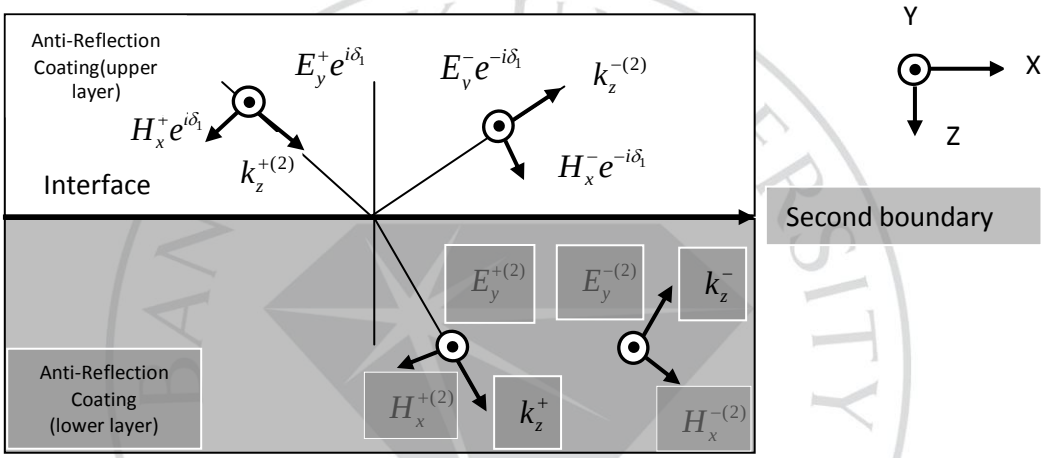

Figure 2.10. Second boundary condition between two dielectric media

Under electric field continuity in the second boundary,

$$E_y^+e^{i\delta_1}+E_y^-e^{-i\delta_1}=E_y^{+(2)}+E_y^{-(2)} \tag{2.54}$$

Again, under magnetic field continuity in the second boundary,

$$H_x^+e^{i\delta_1}+H_x^-e^{-i\delta_1}=H_x^{+(2)}+H_x^{-(2)} \tag{2.55}$$

Now,

$$H_x^+ = k_z^+ \times E_y^+ / \mu w; H_x^- = k_z^+ \times E_y^- / \mu w; H_x^{+(2)} = k_z^{+(2)} \times E_y^{+(2)} / \mu w; H_x^{-(2)} = k_z^{-(2)} \times E_y^{-(2)} / \mu w \tag{2.56}$$

Substituting the value of the equation (2.56) in the (2.55), we get

$$k_z^+ E_y^+ e^{i\delta_1} + k_z^+ E_y^- e^{-i\delta_1} = k_z^{+(2)} E_y^{+(2)} + k_z^{-(2)} E_y^{-(2)}$$

$$k_z^+ (E_y^+ e^{i\delta_1} - E_y^- e^{-i\delta_1}) = k_z^{+(2)} (E_y^{+(2)} - E_y^{-(2)})$$

$$k_z^+ (E_y^+ e^{i\delta_1} - E_y^- e^{-i\delta_1}) = k_z^{+(2)} (E_y^{+(2)} - E_y^{-(2)}) \tag{2.57}$$

Using the equation (2.54) and (2.55) in the matrix form, we get,

$$\begin{bmatrix} e^{i\delta_2} & e^{-i\delta_2} \\ k_z^+ e^{i\delta_2} & -k_z^+ e^{-i\delta_2} \end{bmatrix} \begin{bmatrix} E_y^+ \\ E_y^- \end{bmatrix} = \begin{bmatrix} 1 & 0 \\ k_z^{+(2)} & -k_z^{+(2)} \end{bmatrix} \begin{bmatrix} E_y^{+(2)} \\ E_y^{-(2)} \end{bmatrix} \tag{2.58}$$

Let,

$$C = \begin{bmatrix} e^{i\delta_2} & e^{-i\delta_2} \\ k_z^+ e^{i\delta_2} & -k_z^+ e^{-i\delta_2} \end{bmatrix} D = \begin{bmatrix} 1 & 0 \\ k_z^{+(2)} & -k_z^{+(2)} \end{bmatrix} \tag{2.59}$$

$$\begin{bmatrix} E_y^+ \\ E_y^- \end{bmatrix} = AB^{-1} \begin{bmatrix} E_y^i \\ E_y^r \end{bmatrix} \tag{2.60}$$

Using matrix equation (2.53) and (3.3.29), we get

$$\begin{bmatrix} E_y^{+(2)} \\ E_y^{-(2)} \end{bmatrix} = CD^{-1}AB^{-1} \begin{bmatrix} E_y^i \\ E_y^r \end{bmatrix} \quad \text{or} \quad \begin{bmatrix} E_y^i \\ E_y^r \end{bmatrix} = A^{-1}BC^{-1}D \begin{bmatrix} E_y^{+(2)} \\ E_y^{-(2)} \end{bmatrix} \tag{2.61}$$

Third Boundary Condition:

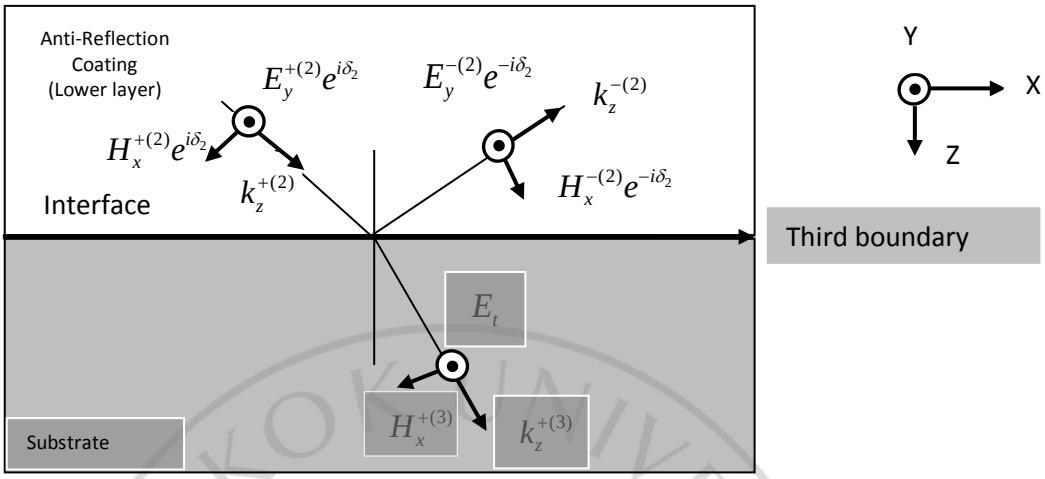

Figure 2.11. Third boundary condition between two dielectric media

Under electric field continuity in the third boundary,

$$E_y^{+(2)}e^{i\delta_2} + E_y^{-(2)}e^{-i\delta_2} = E_t \tag{2.62}$$

Again, under magnetic field continuity in the second boundary,

$$H_x^{+(2)}e^{i\delta_2} + H_x^{-(2)}e^{-i\delta_2} = H_x^{+(3)} \tag{2.63}$$

Now,

$$H_x^{+(2)} = k_z^{+(2)} \times E_y^{+(2)} / \mu w; H_x^{-(2)} = k_z^{-(2)} \times E_y^{-(2)} / \mu w; H_x^{+(3)} = k_z^{+(3)} \times E_t \tag{2.64}$$

Substituting the value of the equation (2.64) in the (2.63), we get

$$k_z^{+(2)}E_y^{+(2)}e^{i\delta_2} + k_z^{-(2)}E_y^{-(2)}e^{-i\delta_2} = k_z^{+(3)}E_t$$

$$k_z^{+(2)}(E_y^{+(2)}e^{i\delta_2} - E_y^{-(2)}e^{-i\delta_2}) = k_z^{+(3)}E_t$$

(2.65)

Using the equation (3.3.31) and (3.3.34) in the matrix form, we get

$$\begin{bmatrix} e^{i\delta_2} & e^{-i\delta_2} \\ k_z^{+(2)}e^{i\delta_2} & k_z^{-(2)}e^{-i\delta_2} \end{bmatrix}\begin{bmatrix} E_y^{+(2)} \\ E_y^{-(2)} \end{bmatrix} = \begin{bmatrix} 1 & 0 \\ k_z^{+(3)} & 0 \end{bmatrix}\begin{bmatrix} E_t \\ E_t \end{bmatrix} \tag{2.66}$$

Let, $E = \begin{bmatrix} e^{i\delta_2} & e^{-i\delta_2} \\ k_z^{+(2)}e^{i\delta_2} & k_z^{-(2)}e^{-i\delta_2} \end{bmatrix}$ & $F = \begin{bmatrix} 1 & 0 \\ k_z^{+(3)} & 0 \end{bmatrix}$

Then,

$$\begin{bmatrix} E_y^{+(2)} \\ E_y^{-(2)} \end{bmatrix} = E^{-1}F\begin{bmatrix} E_t \\ E_t \end{bmatrix} \tag{2.67}$$

Finally, using equation (2.53), (2.61) and (2.67)

$$\begin{bmatrix} E_y^i \\ E_y^r \end{bmatrix} = A^{-1}BC^{-1}DE^{-1}F\begin{bmatrix} E_t \\ 0 \end{bmatrix} \tag{2.68}$$

Equation (2.67) can be simplified as,

$$\begin{bmatrix} E_y^i \\ E_y^r \end{bmatrix} = \begin{bmatrix} m_{11} & m_{12} \\ m_{21} & m_{22} \end{bmatrix}\begin{bmatrix} E_t \\ 0 \end{bmatrix} \tag{2.69}$$

$$E_y^r = E_t m_{21}$$

$$E_y^i = E_t m_{11}$$

$$\frac{E_t}{E_y^i} = \frac{1}{m_{11}}$$

$$t = \frac{E_t}{E_y^i} = \frac{1}{m_{11}} \tag{2.71}$$

where‘t’ is the transmission coefficient amplitude

$$E_y^r = \frac{E_y^i}{m_{11}} m_{21}$$

$$\frac{E_y^r}{E_y^i} = \frac{m_{21}}{m_{11}}$$

$$r = \frac{E_y^r}{E_y^i} = \frac{m_{21}}{m_{11}} \tag{2.72}$$

where ‘r’ is the reflection coefficient amplitude

Alternate T-Matrix Method: Please refer Appendix-II

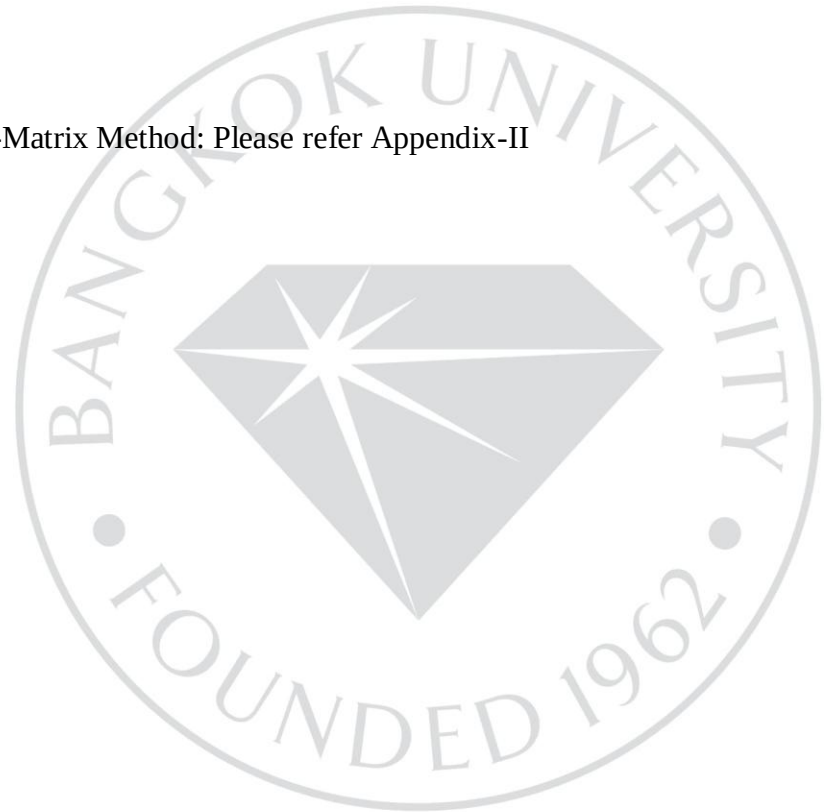

CHAPTER 3

METHODOLOGY

3.1 Research Design

An antireflective coating is synthesis using effective medium composed of porous material with metal nanoparticles embedded as an inclusion in the host. Multilayer antireflection is considered for wide spectrum of reflection minimum. The effective permittivity of the composite ultra thin layer is regulated using the volume fraction tuning between the host material and the inclusion. The desired effective permittivity supports the condition to attain the antireflection property. On varying the concentration of the metal nanoparticle on the top layer of a double layer arrangement with required tuned porosity of the two layers medium the desired antireflection properties is achieved. Here the two different medium of desired refractive index is considered in the two layers of thin film arrangement for the optical broadband as it attains the property of double layer antireflection. The ARC considers double layer thin film structure in order to increase the degree of freedom in designing and ease of fabrication using spin coating. In order to avoid the need of more layers of thin films, a specific refractive index can be attained by the composite material on tuning the concentration ratio of the inclusions in the host medium. It is as well more advantageous to provide such mixing properties to just one layer of the two thin film arrangements as shown in the figure 3.1. Control of the effective permittivity results in the regulation of complex index of refraction relation and thus governing the amount of reflected, transmitted and absorbed light

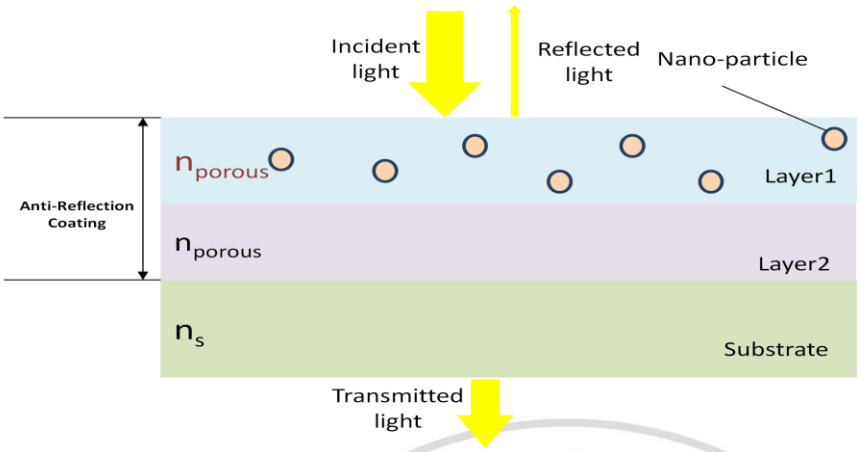

Figure 3.1. Schematic of the proposed diagram.

In order to gain the performance of efficient antireflection coating a desired refractive index of composite material is required. This is sustained by regulating the volume fraction of the nanoparticles inclusion in the host medium or by tuning the porosity of the thin film arrangement. The performance of the thin film can be obtained by calculating the reflectance and transmittance of light using the scattering matrices based on the semi-analytical methods. Once the antireflection property is obtained by the thin film we will look for the broadening of the reflectance minimum along the visible light spectrum. Here, the double layer is designed with a W-type coating to broaden the reflection minimum. This would result in the efficient wide range antireflection coating. However, the ultraviolet parameter has not been considered till now. With the introduction of the metal nanoparticles inclusion in the top layer of the thin film arrangement, the near UV radiation can be partially blocked through the ARC. The blocking range and depth of the UV light can be tuned by regulating the size, shape and the quality of the medium. The

theoretical analysis of the body of methods and principles associated with it is conferred in the flowchart (Refer figure 3.2)

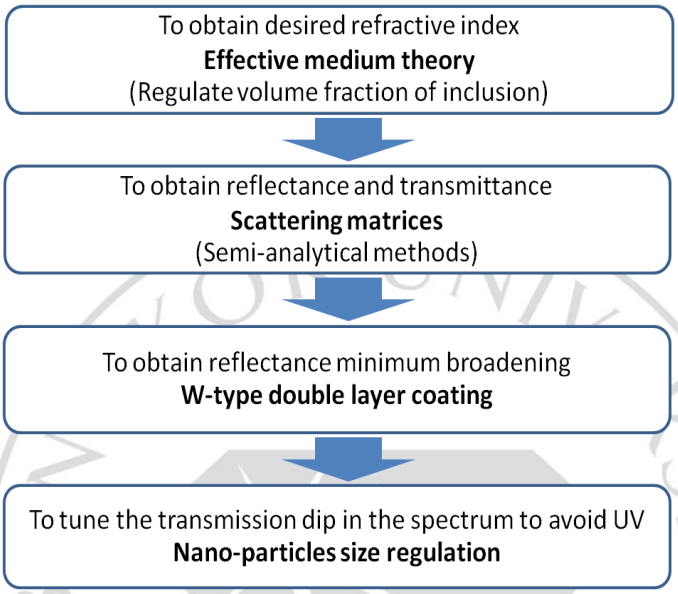

Figure 3.2. Methodology flow chart

3.2 To obtain desired refractive index :

A new effective medium (ε_{MG}) is considered containing inclusion made of two different material, Silver and Titanium dioxide with permittivities ' ε_a ' and ' ε_b ' respectively. The Maxwell Garnett equation under two unlike inclusions in a common host medium is generalized as

$$\frac{\varepsilon_{MG}-\varepsilon_h}{\varepsilon_{MG}+2\varepsilon_h}=f_a\frac{\varepsilon_a-\varepsilon_h}{\varepsilon_a+2\varepsilon_h}+f_b\frac{\varepsilon_b-\varepsilon_h}{\varepsilon_b+2\varepsilon_h} \qquad (3.1)$$

where, f_a and f_b are the volume fractions of the individual inclusions contained by the host medium with dielectric function of air (ε_h). Silver is considered along with the Titanium dioxide as the inclusion in the air as the host medium. The plasmonic resonance properties for the absorption of near UV radiation can be attained using silver nanoparticles within TiO2 based porous thin film for antireflection property.

As per the required application, the reflectivity has to be low along a broader visible light spectrum. The consequence of reflectivity with the change in the thickness of double layer arrangement has not been taken into consideration until now. Appropriate thickness of the two layers in conjunction with the relevant refractive index would result in the quarter wavelength condition. The quarter wavelength condition under optimum coating thickness and reflective index would result to antireflection phenomenon. A multilayer coating design structure termed as V-coating is considered where two layers of quarter wavelength thickness are stacked one over the other to broaden the reflection minimum along the visible spectrum.

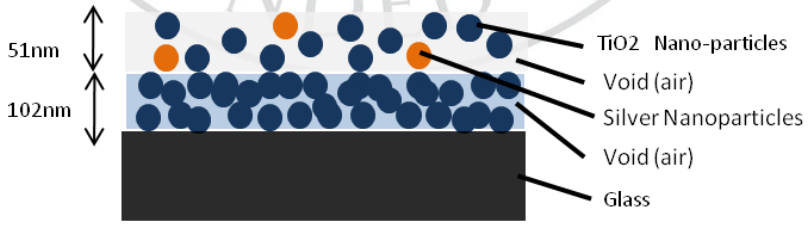

Figure 3.3. Schematic view of double layer ARC with TiO2 and silver nanoparticles as inclusion in the air host on the top layer.

In order to achieve reflection reduction along a broader spectrum of light wave, a better multilayer coating design structure termed as W-coating(Musset & Thelen, 1970) is developed. The W-type coating is designed in such a way that for two layer arrangement the upper layer is half wave film and the lower layer is quarter wave film layered over a substrate(D. E. Aspnes, 1982a). As the antireflection properties is desired along the span of the visible light spectrum W-coating is considered with the top layer thickness of 51nm and the bottom layer thickness of 102nm as shown in figure 3.3.

Volume Fraction effect:

In the present sub-division, the effective dielectric response of heterogeneous composite thin film structure is studied in terms of transmissivity. The proposed thin film arrangement has material with two different polarizability α_a (TiO2) and α_b (Silver) in the air host medium. By repeating the Maxwell-Garnett under multi-component mixture, we find

$$\frac{\varepsilon_e - 1}{\varepsilon_e + 2} = \frac{4\pi}{3}(\mathbf{n}_a \alpha_a + \mathbf{n}_b \alpha_b) \tag{3.2}$$

where ε_e is the effective dielectric function of the complex medium. The Lorentz-Lorenz effective medium expression shown in equation (3.3) is considered as the pure forms of the dielectric function for each of the phases ‘a’ and ‘b’ are available.

$$\frac{\varepsilon_e - 1}{\varepsilon_e + 2} = f_a \frac{\varepsilon_a - 1}{\varepsilon_a + 2} + f_b \frac{\varepsilon_b - 1}{\varepsilon_b + 2} \tag{3.3}$$

where, $f_{a,b} = n_{a,b}/(n_a + n_b)$ are the concentration i.e volume fractions of the corresponding phases ‘a’ and ‘b’, respectively. The inclusions in the range of nano-scale size should

retain their dielectric identity within the host medium. Here, the two different inclusion is embedded with the vacuum (ε = 1) as the host medium. Considering the host dielectric function is ε_h, then eqn. (3.3) becomes

$$\frac{\varepsilon_e - \varepsilon_h}{\varepsilon_e + 2\varepsilon_h} = f_a \frac{\varepsilon_a - \varepsilon_h}{\varepsilon_a + 2\varepsilon_h} + f_b \frac{\varepsilon_b - \varepsilon_h}{\varepsilon_b + 2\varepsilon_h} \tag{3.4}$$

The concentration of the inclusions would direct the change in the volume fraction, $f_{a,b}$. With the change in the concentration of the silver nanoparticles in one of the layer in the proposed thin film structure, there exist a drop in the transmission dip over a particular range of wavelength. The transmission dip is more pronounced with the increase in the volume fraction of the metal nanoparticles inclusion.

The decrease in the transmitted light energy is prominent in the wavelength ranging from 340nm-370nm. It is evident from the previous study that with the increase in the volume fraction of metal particles, the absorption of light is more predominant near UV range. As absorption of light energy increases within a body, the corresponding transmission energy drops down accordingly.

3.3 To obtain reflectance and transmittance

In order to calculate the scattering of electromagnetic waves by stacks of multilayer films, Transfer- matrix method based on plane-wave has been normally came into play. However, based on semi-analytical method a new and enhanced formulation (Rumpf, 2011) of scattering matrices is considered which is reliable with existing convention and effective in execution under constrain memory allocation. Semi-

analytical method is considered as a desired computational method as our proposed structure is represented as a stack of multiple layers with varying thickness and reflective index. The complexity of the electromagnetic field exists along the transverse plane of each layer of the multilayers thinfilm structure whereas the field is uniform along the longitudinal direction.

On eliminating E_z and H_z , which are the longitudinal field component in the expanded Maxwell's equations under the condition of normalized magnetic field using back substitution gives matrix form (L. Li, 1996),

$$\frac{\partial}{\partial z}\begin{bmatrix} e_x \\ e_y \end{bmatrix} = k_0 P \begin{bmatrix} \tilde{h}_x \\ \tilde{h}_y \end{bmatrix} \tag{3.5}$$

$$\frac{\partial}{\partial z}\begin{bmatrix} \tilde{h}_x \\ \tilde{h}_y \end{bmatrix} = k_0 Q \begin{bmatrix} e_x \\ e_y \end{bmatrix} \tag{3.6}$$

Based on the Yee grid (Schneider & Kruhlak, 2001) the field components are present in the column vector mentioned as $e_x, e_y, \tilde{h}_x \; and \; \tilde{h}_y$ at the discrete point throughout the transverse plane.

Differentiating the equation (3.5) with respect to 'z' and substituting in equation (3.6) would result in a matrix wave equation with normalizing 'z' as

$$\frac{\partial^2}{\partial z'^2}\begin{bmatrix} e_x \\ e_y \end{bmatrix} - \Omega^2 \begin{bmatrix} e_x \\ e_y \end{bmatrix} = \begin{bmatrix} 0 \\ 0 \end{bmatrix} \tag{3.7}$$

$$\Omega^2 = PQ \tag{3.8}$$

$$\psi(z') = \begin{bmatrix} e_x(z') \\ e_x(z') \\ \tilde{h}_x(z') \\ \tilde{h}_x(z') \end{bmatrix} = \begin{bmatrix} W & W \\ -V & V \end{bmatrix} \begin{bmatrix} e^{-\lambda z'} & 0 \\ 0 & e^{\lambda z'} \end{bmatrix} \begin{bmatrix} C^+ \\ C^- \end{bmatrix} \tag{3.9}$$

$$V = QW\lambda^{-1} \tag{3.10}$$

W contains the eigen-modes of the electric field

V contains the eigen-modes of the magnetic field.

$e^{-\lambda z'}$ describe the forward propagation through layers

$e^{\lambda z'}$ describe the backward propagation through layers

C^+ amplitude coefficient of the eigen-modes (forward directions)

C^- amplitude coefficient of the eigen-modes (backward directions)

Using scattering matrices, the boundary condition can resolved considering one layer at a time. Based on the scattering matrix a layer (say x) can be defined as

$$\begin{bmatrix} c'^{-}_{1} \\ c'^{+}_{2} \end{bmatrix} = \begin{bmatrix} S^{(x)}_{11} & S^{(x)}_{12} \\ S^{(x)}_{21} & S^{(x)}_{22} \end{bmatrix} \begin{bmatrix} c'^{+}_{1} \\ c'^{-}_{2} \end{bmatrix} \tag{3.11}$$

$S^{(x)}_{11}$, $S^{(x)}_{12}$, $S^{(x)}_{21}$ and $S^{(x)}_{22}$ are the square matrices which describe the scattering parameters. The scattering parameter describes the energy dispersed among the individual eigen-modes. The mode coefficients right outside the layers is present in column vectors $c'^{+/-}_{1/2}$ as show in the figure 3.4.

Considering the first boundary condition at the interface between the air and the upper layer of the ARC, the expression for the scattering parameter is

$$\begin{bmatrix} W_{air} & W_{air} \\ V_{air} & -V_{air} \end{bmatrix} \begin{bmatrix} c'^{-}_{air} \\ c'^{+}_{air} \end{bmatrix} = \begin{bmatrix} W_1 & W_1 \\ V_1 & -V_1 \end{bmatrix} \begin{bmatrix} c'^{+}_{1} \\ c'^{-}_{1} \end{bmatrix} \tag{3.12}$$

And for the second boundary condition between the top layer and the bottom layer of ARC, scattering parameters are expressed as

$$\begin{bmatrix} W_1 & W_1 \\ V_1 & -V_1 \end{bmatrix} \begin{bmatrix} e^{-\lambda_1 k_0 L_1} & 0 \\ 0 & e^{\lambda_1 k_0 L_1} \end{bmatrix} \begin{bmatrix} c'^{+}_{1} \\ c'^{+}_{1} \end{bmatrix} = \begin{bmatrix} W_2 & W_2 \\ V_2 & -V_2 \end{bmatrix} \begin{bmatrix} c'^{+}_{2} \\ c'^{-}_{2} \end{bmatrix} \tag{3.13}$$

Combining the equation (3.12) and (3.13) and rearranging the terms in the form of equation (11), we can derive all the scattering matrix elements.

As we have considered double layer thin film there exist two scattering matrix say, $S^{(1)}$ followed by $S^{(2)}$, the resultant scattering matrix is $S^{(12)} = S^{(1)} \otimes S^{(2)}$, using the star product (Redheffer, 1961) represented as

$$\begin{bmatrix} S_{11}^{(12)} & S_{12}^{(12)} \\ S_{21}^{(12)} & S_{22}^{(12)} \end{bmatrix} = \begin{bmatrix} S_{11}^{(1)} & S_{12}^{(1)} \\ S_{21}^{(1)} & S_{22}^{(1)} \end{bmatrix} \otimes \begin{bmatrix} S_{11}^{(2)} & S_{12}^{(2)} \\ S_{21}^{(2)} & S_{22}^{(2)} \end{bmatrix} \tag{3.14}$$

Where the resultant value turns out to be

$$S_{11}^{(12)} = S_{11}^{(1)} + S_{12}^{(1)} \left[I - S_{11}^{(2)} S_{22}^{(1)} \right]^{-1} S_{11}^{(2)} S_{21}^{(1)} \tag{3.15}$$

$$S_{12}^{(12)} = S_{12}^{(1)} \left[I - S_{11}^{(2)} S_{22}^{(1)} \right]^{-1} S_{12}^{(2)} \tag{3.16}$$

$$S_{21}^{(12)} = S_{21}^{(2)} \left[I - S_{22}^{(1)} S_{11}^{(2)} \right]^{-1} S_{21}^{(1)} \tag{3.17}$$

$$S_{22}^{(12)} = S_{22}^{(2)} + S_{21}^{(2)} \left[I - S_{22}^{(1)} S_{11}^{(2)} \right]^{-1} S_{22}^{(1)} S_{12}^{(2)} \tag{3.18}$$

As seen from the figure2 the thin film arrangement is existing between the air(reflection region) and the substrate(transmission region), hence the final scattering matrix, S_{globel} is represented as

$$S^{(global)} = S^{air} \otimes S^{12} \otimes S^{substrate} \tag{3.19}$$

A connecting matrix is generated between the mode coefficient of the reflected (c_{ref}) and transmitted wave (c_{trn}) to the mode coefficient of the incident wave (c_{inc}). This matrix which relates the two matrices is termed as global scattering matrix as shown below:

$$\begin{bmatrix} c_{ref} \\ c_{trn} \end{bmatrix} = \begin{bmatrix} S_{11}^{globel} & S_{11}^{globel} \\ S_{11}^{globel} & S_{11}^{globel} \end{bmatrix} \begin{bmatrix} c_{inc} \\ o \end{bmatrix} \tag{3.20}$$

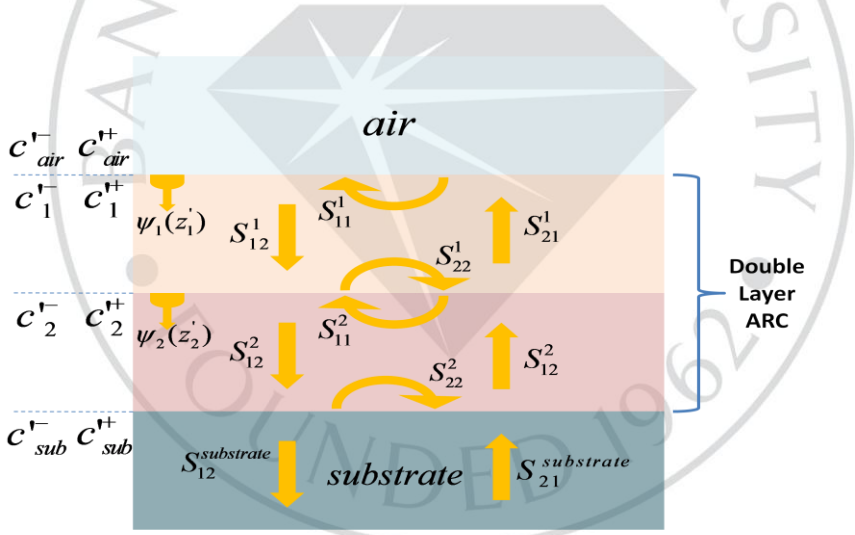

Figure 3.4. Mathematical framework for combining two scattering matrix representing ARC

The electromagnetic field on connecting with the corresponding mode coefficient, the reflecting and transmitting wave for each specific wavelength over the entire range of visible light can be obtained for the double layer ARC. The effective medium engineered

with the metal nanoparticle inclusion deduced using the Maxwell Garnett model along with the property of the metal nano-particle has been substituted in the scattering matrix computational technique to obtain the intensity of the transmitted light considering the dispersive property of the material. It is required to deduce reflection minimum under a broad visible light spectrum along the blue light region. In the current subdivision of the chapter, the discussion on the subject of attaining antireflection property using quarter wavelength of double layer coating has not been discussed. There exist a range of techniques to attain broadband antireflection properties along the visible light spectrum with the help of varying the width of thin film coating. The width of the two layer are regulated in such a way that reflection minimum is achieved.

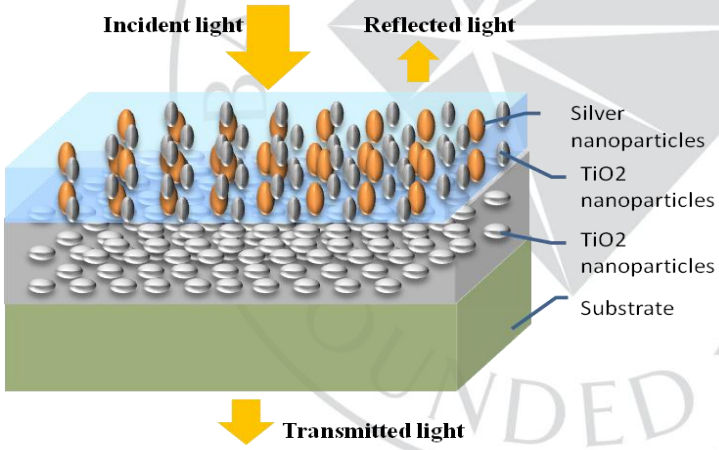

Figure 3.5. Schematic diagram of the proposed structure

Top layer (51 nm thickness) : Silver & Titanium dioxide as the inclusion in the air base medium.

Bottom layer (102nm thickness) : Only Titanium dioxide as the inclusion in the air base medium.

The plasmonic properties for the absorption of near UV radiation can be attained using silver nanoparticles with TiO2 based porous thin film for antireflection property.

3.4 To obtain Reflectance minimum broadening

With the emergence of advanced engineered material and complexity in the deposition method of ultra thin film have supported sophisticated multilayer design of AR coating. The increasing demand of high efficient solar cell in the field of solar industries has fueled further demand of ARC coating. In the early years, the concept of gaining the AR property was to attain the condition of quarter-wave or half-wave layers where the optical thicknesses(thickness with relative permittivity) of the layers were an multiple of a quarter of the design wavelength.

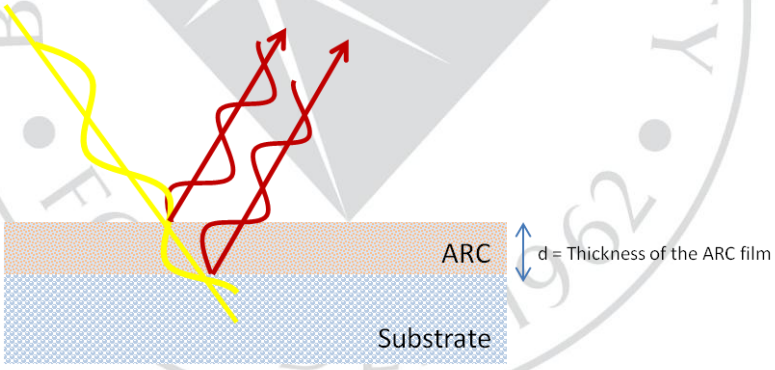

Figure 3.6. Interference of light reflected from the two interface of a single layer antireflection coating

The design philosophy to achieve the property of anti-reflection in a thin film coating is to regulate the permittivity of film and corresponding optical thickness so that destructive interference occurs between the reflected light rays. In order to achieve

destructive interference for anti-reflection property a central wavelength has to choose where the maximum dip in the reflectivity will be observed. This reduction in the reflectivity for a broader spectrum can be attained by using multiple coating layers

In the early years of the thin film deposition technique the multilayer thinfilm design was restricted to three to four layers. This was because it was relatively simple to fabricate and examine the deposition of quarter-wave or half-wave thinfilm stacks. Under limited number of layers it is inadequate to achieve notable antireflection property for a broader light spectrum as material of preferred refractive indices is hard to find in nature. The antireflective property of a thinfilm arrangement is highly sensitive to the slight change in the reflective indices of the material. In the need to optimize the performance of system in the optical domain and in the field of advance thinfilm technology, there has always be a urge for improving the antireflective property beyond the range attainable by a single layers coating (4% reflectance for bare glass). Further reduction in reflectivity can be achieved by engineering new composite material with design structure and increasing the number of layers over the substrates.

Although the coating reduces the reflectance substantially there are two major deficiencies:

1. The residual reflectance at the minimum is not low enough for many applications;
2. While the reflected light from the coated surface leads to coloring, the uncoated surface is neutral in color.

However the second statement does not pose any effect to our application.

The following ways are mentioned below to improve the antireflective property of a single layer thin film arrangement:

1. Regulating the permittivity of the composite material and its thickness (inhomogeneous antireflection coatings) or
2. Fabricating stacks of multilayer thinfilm with dissimilar permittivity(multilayer antireflection coatings).

In the present scenario, multilayer AR coating has wide application in the field of ophthalmic lens technologies. However, inhomogeneous antireflection coatings are still in the experimental state as a result of the complexity in the design of composite medium. Keeping in view of this condition we shall limit the design methodology of the antireflection thin film to homogeneous multilayer arrangement.

The literature on antireflection coatings is extremely widespread and diverged. Here has not been made much attempt to trace the various design methodology in support of attaining AR property in a thin film structure historically. We shall expose ourselves within the limit of current design methods which attains practical relevance. In practical scenario all material does absorb light to an extent. Therefore, throughout the computational approach absorption property with the dispersion effect of the subjected material is considered. In general, we consider normal light incidence over the parallel plane surface of the AR coating. There exit a limitation in the selection of material to be used in the fabrication of thin film for antireflection coating. Very few materials in nature support the fine layering of thin film.

Two-Layer Antireflection Coating:

There exist ingenious methods of layering of thin film which can optimize the antireflective property of at a broader light spectrum. There are certain established designs in the layering of thin film which has been verified to be finest in its class of attaining antireflection property. Usually simple design method is adopted while fabricating multiple layers for the ease of fabrication. Adopting a specific design method for optimal antireflective property is arbitrary and highly individual as it is based on the problem that has to be addressed.

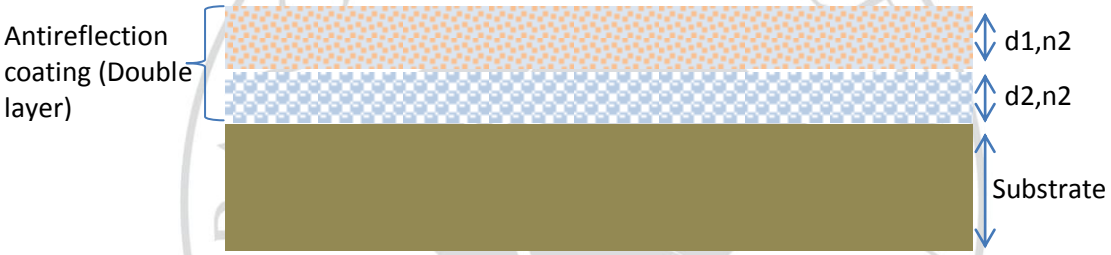

Figure 3.7. Schematic for double layer thin film coating over a substrate

From the given figure, it is fairly clear that the reflectance of the light from the double layer coating can be varied with the change in the reflective index and the thickness of the two layers. Within the spectrum of visible light there can be a substantial change in the reflectance which can be tuned to the required application for our project.

There are two types of design structure under double layer antireflection coating which will prevent the reflection of light through specific width of spectral band. V-type coating design (double layers of quarter wavelength thickness is coated over a glass substrate) helps in reduction of reflection at a narrow spectral band. The next is the W-

type coating which will support of reflection reduction at a broader spectral band (Macleod, 1986). In W-type coating, a thin film with the thickness of half of the applied wavelength ($n_2d_2 = \lambda/2$) is coated between a quarter wave thin film ($n_1d_1 = \lambda/4$) and the substrate (D. E. Aspnes, 1982b) as shown in the figure 3.8.

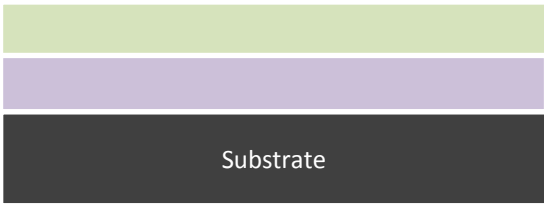

Figure 3.8. Condition for double layer w-type antireflection coating.

The comparative result between W-type and V-type coating observed from the figure 3.9 have clearly affirmed that W-type coating give way a broader reflectance minimum. As per the requirement, the W-type coating design is considered as the reflectance should be least all along the visible light spectrum.

Broadening of the reflection minimum can be achieved along the large spectrum of visible light by the so-called W-coating arrangement for double layer antireflection coating. For even distribution of the minimal reflectance along the visible spectra 510nm is consider to the mean value of reference. The thickness is based on the relation between the refractive index at a particular wavelength as stated, $n \times d = \lambda / 4$. Here, the thickness of the lower layer is based on the relation of, $d_2 = \dfrac{\lambda}{\eta_2 \times 2}$, where $\lambda = 510nm$.

The change in the reflective properties of the proposed thin film arrangement is observed from the figure 3.10 while changing the refractive index of the bottom layer.

The refractive index of the upper layer of the AR coating is considered to be fixed at 1.38 (this value is based in general on the refractive index of MgF2 at 500nm wavelength). Let us assume that the index of refraction for the substrate is 1.6. With the lower layer and upper layer to be 1.38 and 1.7 respectively, the minimum reflectance broadening is observed among the three waveforms.

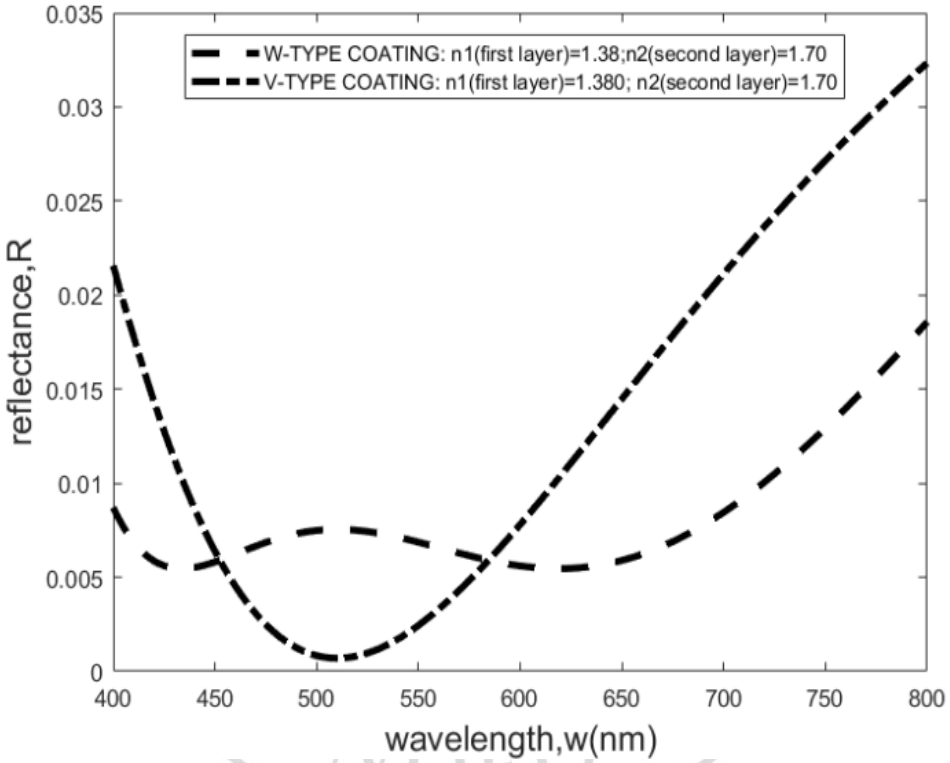

Figure 3.9. Reflectance of various two-layer coating on a substrate with substrate index (ns)=1.6 and medium index(no)=1.0(air);4n1d1=510nm (top layer) , 4n2d2=1020(bottom layer) .

3.5 To tune the transmission dip in the spectrum to avoid UV

A band of electrons collectively oscillates to generate localized surface plasmon resonance (LSPR) which results in the enhancement of the electromagnetic (EM) field at the metal nano-particle surface shown in figure 3.11. As metal nanoparticles are embedded in the complex dielectric host medium a leading enhancement mechanism of surface-enhanced Raman scattering (SERS) comes into existence, termed as Localized surface plasmon resonance (LSPR) (Kneipp et al., 2006) (Ru & Etchegoin, 2008) (Andrews et al., 2010). Because of the increase in the EM near field among the molecules on the metal surface the scattering is more efficient which helps in the release

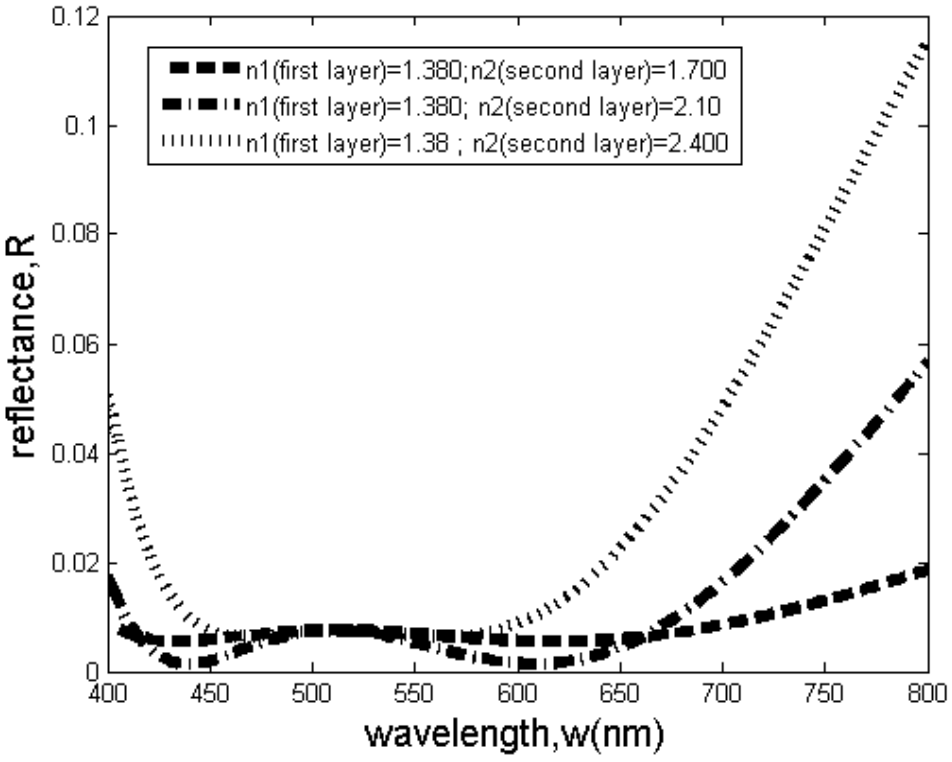

Figure 3.10. Reflectance of various two-layer w-type coating on a substrate with substrate index (ns)=1.6 and medium index(no)=1.0(air);4n1d1=510nm (top layer), 4n2d2=1020(bottom layer).

of energy in the form of absorption.

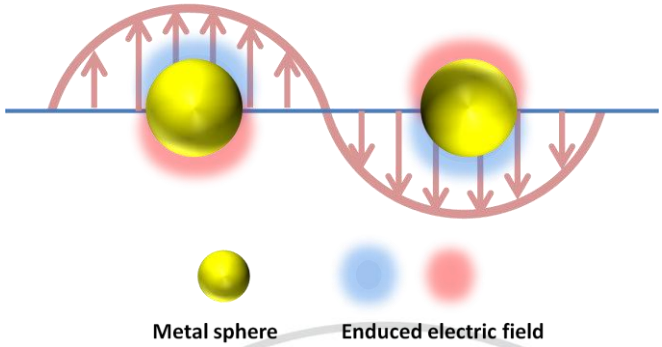

Figure 3.11. Illustration of the excitation of localized surface plasmon resonance

In general, the plasmon resonances in the metal are more prominent along the region of visible light spectrum. Hence, the SERS effect is usually exhibited towards the visible and near infra-red light region. The substrates normally display small EM enhancement when subjected to the UV radiation. This effect is observed due to damping caused by the interband transitions (Palik, 1998). Silver nanoaprticles display enhanced plasmon resonances along the blue light region and near-UV region. Metal nano-particles made of metals like Ag, Au, Al, Cu, Zn and In exhibit SERS (Tian et al., 2006). It is required to have the SERS effect in the region of ultra violet and in particular near ultraviolet region to prevent the transmission of light under the affirmed region.

Figure 3.12. Spectral region of desired SERS effect for near UV blocking.

As we focus on the absorption of near-UV light to prevent it to filter through the substrate certain metal nano-particles of specific shape and size is considered. These metal particles will be designed to acts as SERS substrate which will enhance the Raman signal in the range of high frequency visible light spectrum hence prevent it to filter through the thin film coating.

Varying Metal Composite and Impending Conditions :

There exist discrete metallic particles with plasmonic effect (David E. Aspnes, 1982) which are increasingly being incorporated into various technologies and engineering products. Plasmonic effect in an optical material is observed because of the conduction electron in the atoms collectively oscillates to produce intense amplification of the electric field at the periphery of the nanomaterial. A localized surface-plasmon resonance is generated in the vicinity of the metal nanoparticles with the interaction with the dielectric host medium. This high resonant or near resonant outcome has been established with a number of molecules and many metals, including Cu, Ag, Au, Li, Al, K, In, Zn, Pt and Rh.

The plasmonic effect is acknowledged in various metals on both electrodynamic modeling using spheroids and experimental studies. However, there is ambiguity about the existence and effect of the metal size in the application of antireflection property on various metals. Therefore an electromagnetic theory calculation will facilitate a benchmark to analysis the significance of experimental results under various metals. Several metal based on its availability and recent interest in plasmonic effect is considered which includes Ag, Au, Al, Cu, Zn and In. Based on the earlier studies, metal

nanoparticles made of metals like Ag, Au and Cu exhibit intense plasmonic effect (Ferry et al., 2010) in the visible light region. It is required to have the plasmonic effect in the region of ultra violet and in particular near ultraviolet region to prevent the transmission of light under the affirmed region.

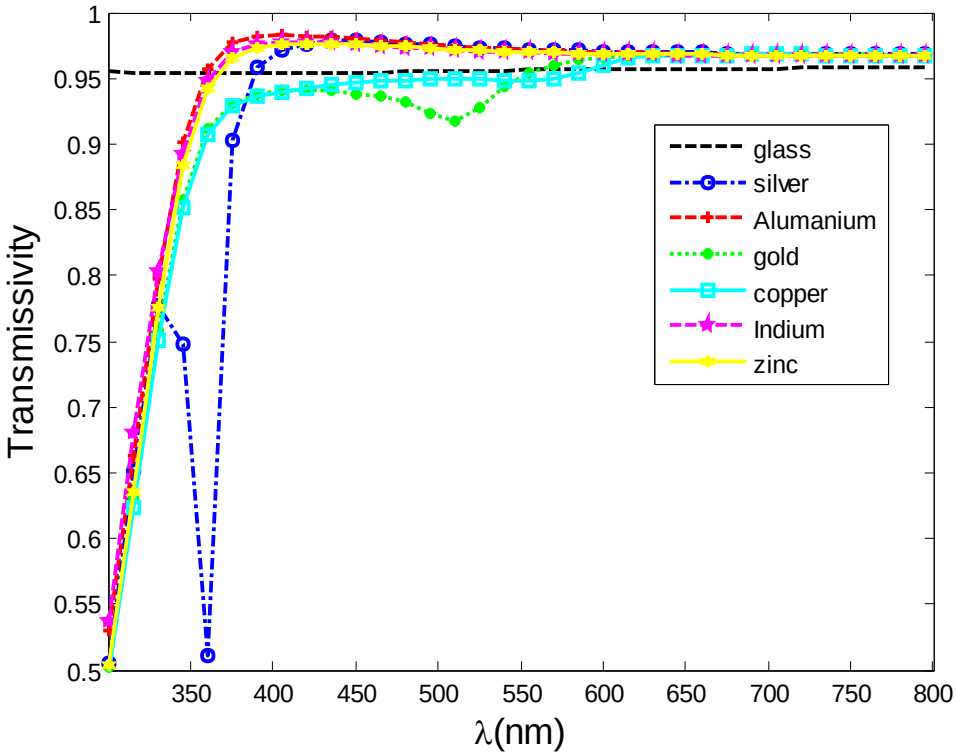

Figure 3.13. Transmissivity under various metal nanoparticles inclusion in the thin film arrangement

In order to find the plasmonic effect of various metal nanoparticles in layers of thin film, they are considered as inclusion in the top layer of a double layer thin film antireflection coating. It is clear from the figure 7 that when the silver nanoparticles is embedded within the upper layer of the double layer arrangement, there exist a spiky dip in the transmitted light near UV region (340nm-380nm). All the aforementioned

nanoparticles are spherical in shape of diameter 10nm. For the gold nanoparticles there exist a shallow dip is the transmission under the higher wavelength(450nm-500nm) of visible light spectrum.

However, the performance of the copper nanoparticles inclusion is below the standard glass coating reference in terms of transmittivity through the silicon substrate. Aluminum shows the better transmittivity to an average of 98 percentages. Al is followed by In and Zn, whose performance is better than the silver under the extended range of 330nm to 410nm. However, the effect of plasmon resonance is not evident in the required range for the light spectrum for Al, In and Zn. Therefore under the stated shape and size, silver is the desired metal which supports in the absorption of light under near-UV light.

CHAPTER 4

FINDINGS

4.1 Hypotheses Findings

The uses of gold and silver nanoparticles were proposed to absorb the ultraviolet radiation along the near UV light during the initial stage. Along with the absorption properties of metal nano-particles(NPs) dues to plasmonic effect, the effective index of two dielectric layers coating can be tuned to gain the anti-reflection property. To devise a thin film structure with desirable optical properties is proposed using metal nanoparticles inclusion embedded within composite host materials. At the initial stage, two layers of thin film coating was assembled where the top layer is MgF_2 (magnesium fluoride) and the bottom layer is PMMA (Polymethylmethacrylate). The transmission spectrum is studied while embedding the metal nanoparticles in the bottom layer of the proposed arrangement on regulating the following parameters

i) Regulating the volume fraction of the composite material in both the layers of the thin film arrangement

ii) Tuning the size of the metal nanoparticles

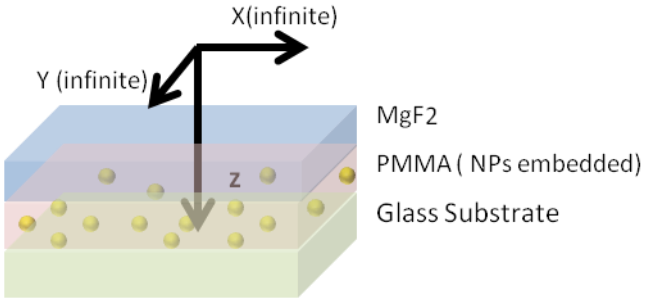

Figure 4.1. Schematic diagram of initially proposed ARC.

On considering the double layer antireflection coating with upper layer as MgF2 (92 nm thickness) and lower layer as PMMA (184 nm thickness) host with silver nanoparticles inclusion over the silicon substrate, it has been observe that as the concentration of the nanoparticles changes the transmitted light get effected. Figure 4.1 shows that as the size of the nanoparticles increases there is a blue shift in the resonance peak of the transmitted light intensity along its wavelength. Moreover, there is a gradual dip in the intensity of the transmitted light along the wavelength with the increase in size of Silver nano-particles which is not evident in Gold nano-particles (as observed from figure 4.2).

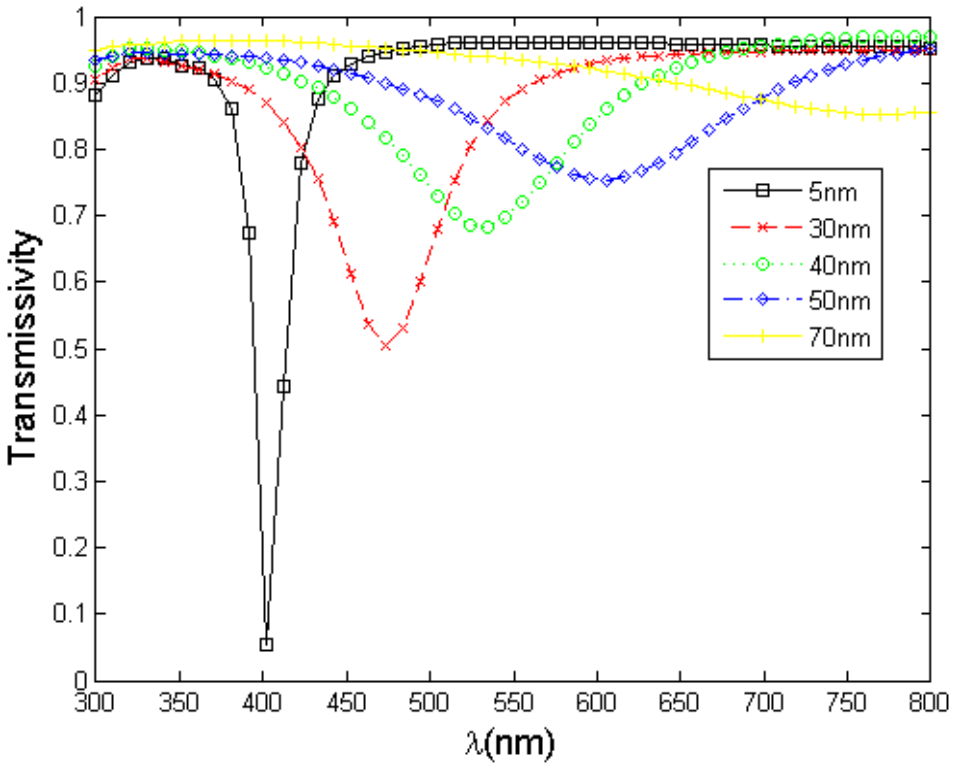

(a)

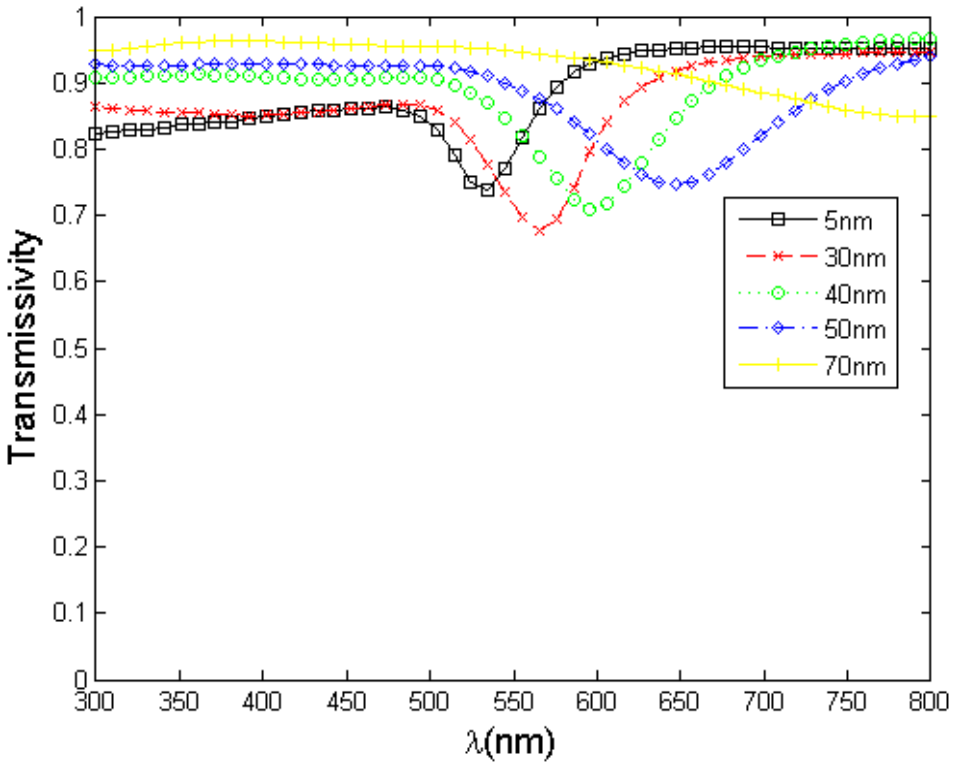

(b)

Figure 4.2. Size variation effect of nanoparticles over the transmitted light through the antireflection coating. (a)inclusion : Silver (b) inclusion : Gold ; Host : PMMA; Volume Fraction:0.01.

The enlargement of the nanoparticles inclusion in the host medium results in the shift of the transmission dip towards the red spectrum color. The peak absorption spike along the visible light spectrum can be shifted towards the preferred wavelength by tuning the nanoparticle size. Under the proposed structure minimum reflection of light is observed when the silver nano-particle of 50nm in size comprises within the concentration ranging from 0 .001 to 0 .05 volume fraction in the dielectric host medium.

As the concentration of the metal nanoparticles increases in the bottom layer of the thin film coating the transmission dip broadens. Based on the curves shown in the figure 4.3, the increase in the volume fraction assists in the wide absorption spectra compromising the antireflective property along the visible light spectra. Therefore it is recommended to have lower volume fraction resulting in sharp absorption peak in the near-UV light and high transmission along the visible light spectrum. As shown in figure it is evident that with volume fraction of 0.001 results in sharp dip which supports in the efficient antireflection properties in the visible light spectrum.

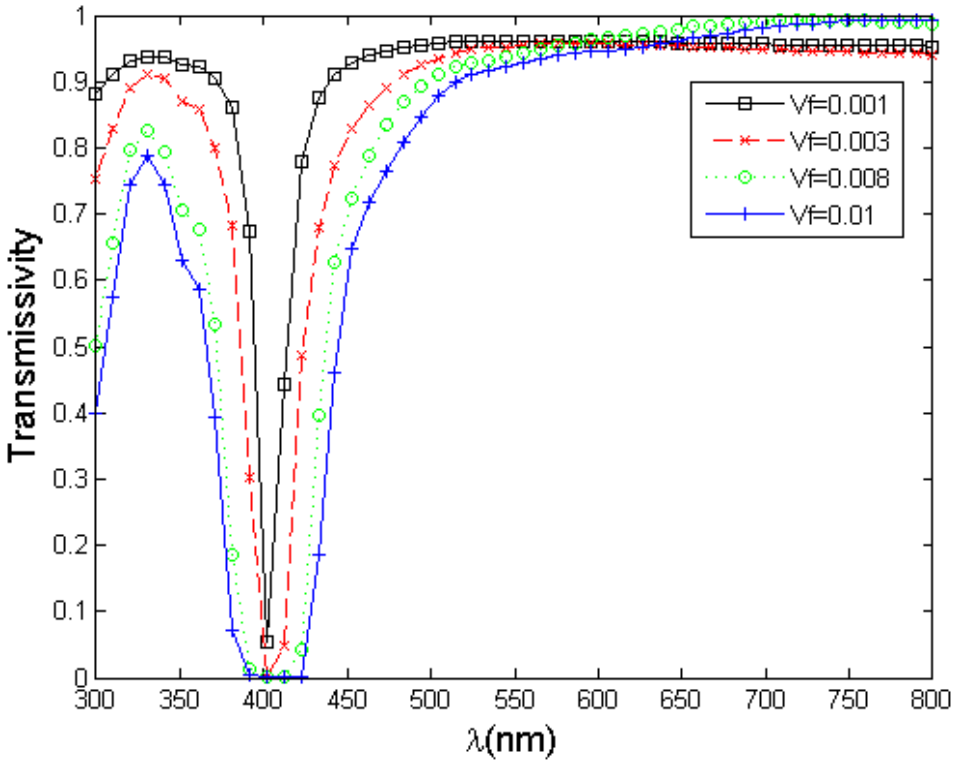

Figure 4.3. Effect of volume fraction of composite material over the transmitted light through the antireflection coating. (a) Inclusion: Silver (b) Inclusion: Gold; Host : PMMA; Nano-particle size: 5nm.

As per the above discussion it is clear that the transmitted light has an effect with the change in the size of the nanoparticles. Moreover, the effect of the concentration of the nano size particulates within the complex medium is depicted in the volume fraction of the inclusion. Using the two parameters of the nano inclusion, i.e, tuning the nanoparticle size and the concentration of the metal nonoparticles, we can regulate the optical property of the material to achieve the effective anti-reflective property.

4.2 Other Findings

Nano-Particle Size and Shape Effect :

Considering the size of the particles in the range of Rayleigh limit, the relation between the permittivity of the material to its polarizability, α is given by (Fleischmann et al., 1974) (Zeman & Schatz, 1987) (*Abhandlungen Über Die Mechanische Wärmetheorie. by Clausius, R.*, n.d.)

$$N\alpha = \frac{3}{4\pi}\frac{\varepsilon - 1}{\varepsilon + 2} \tag{4.1}$$

Where N is the number density for one particle and ε is the dielectric constant. Based on the Maxwell relation $n = \sqrt{\varepsilon\mu} \approx \sqrt{\varepsilon}$ (non-magnetic material is considered), the Lorentz-Lorenz relation gives

$$\alpha = \frac{3}{4\pi}\left(\frac{n^2 - 1}{n^2 + 2}\right)V = \left(\frac{n^2 - 1}{n^2 + 2}\right)a^3 \tag{4.2}$$

where V is the volume and ‘a’ is the radius of the sphere. The effect of the size can be realized from the relationship between the polarizability with the extinction cross-section (Bird, 1964), as stated below

$$\sigma_{ext} = \sigma_{sca} + \sigma_{abs} \tag{4.3}$$

$$\sigma_{ext} = \frac{2\lambda^2}{3\pi}\alpha^6 \left|\frac{m^2-1}{m^2+2}\right|^2 + \frac{-\lambda^2}{\pi}\alpha^3 \operatorname{Im}\left\{\frac{m^2-1}{m^2+2}\right\} \tag{4.4}$$

The extinction cross section is a function of the particles size ‘a’, the property of the material inclusion ‘m’ (refractive index) and the property of the host material ‘m_0’ (refractive index) .

Here, $\alpha = \frac{2\pi a}{\lambda}$, a dimensionless unit parameter and $\lambda = \frac{\lambda_0}{m_0}$ where λ_0 is the incident wavelength in vacuum. , and m_0 represents the refractive index of the host medium which is air. As the material parameter (inclusion and host medium) and size is considered within the expression of extinction cross section the absorption behavior under a specific wavelength differs with the change in size and material composition.

The dependence of size variation of silver inclusion on the transmittance is studied in the figure 4.4. As the size of the nanoparticles increases, the transmissivity curve experiences red shifts in the transmission dip. In our application it is preferred to have the size of metal nanoparticles below 10nm for a sharp transmission dip in the range of near UV radiation.

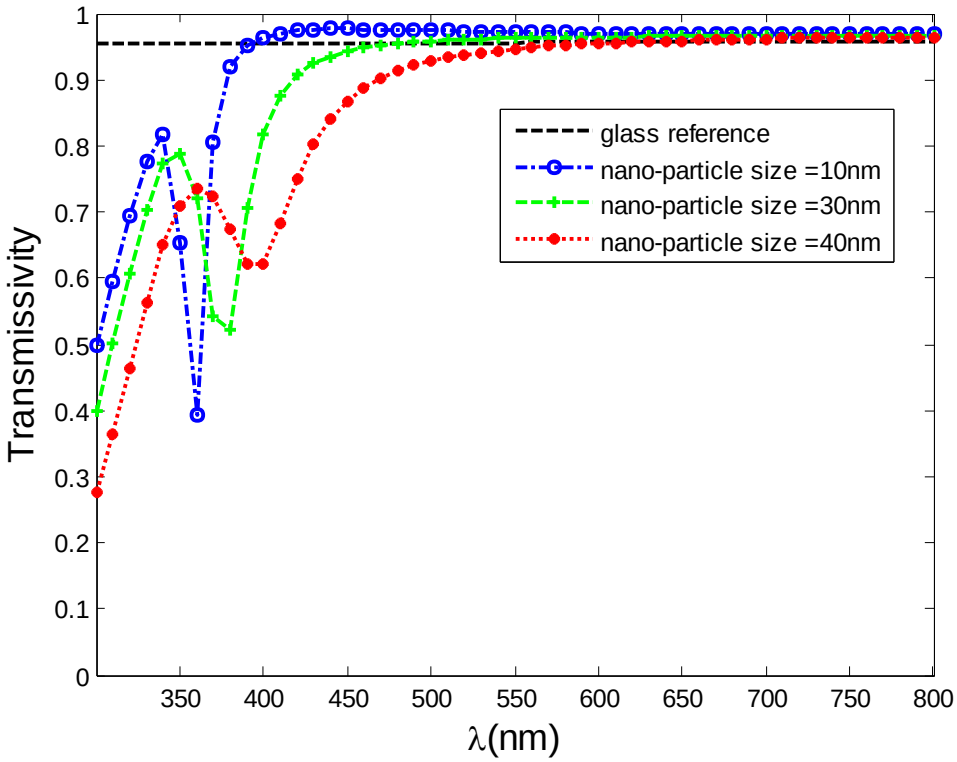

Figure 4.4. Size effect of silver nanoparticles inclusion on transmissivity.

There are significant modifications in the electromagnetic enhancement effect that the new geometry can brings about when a ray of light is subjected on nonspherical metal particle. The plasmonic resonance of molecules placed near the tip of prolate ellipsoids or near the waist of oblate ellipsoids is enhanced. Since the enhancement is largest in the region of the highest curvature, the plasmonic resonance on the surface will be dominated by molecules adsorbed near the tip of prolate. When surrounded by an ambient medium of dielectric constant greater than unity, the plasmon resonance shifts further to the red. Even metals that are not innately good plasmon enhancers are predicted to produce sizable plasmonic signals, provided one can produce colloidal particles or surface features of sufficiently large aspect ratio. Simple dipolar coupling predicts a red shift in

the plasmon resonance frequency with increasing packing density and an overall increase in the intensity of the resonance.

In general, Maxwell-Garnett theory does not address the shape and size effect of the particles in the composite material, as the dimension of the particles is consider much smaller then wavelength of the incident light (Mossotti, 1846). However, under dynamic MG the screening parameter *K* is governed by particle shape and size. The Lorentz depolarization factor is a function of the shape of the particle. The depolarization factor (Hornyak et al., 1997) with field along the minor axis is given by

$$q_b = \frac{1-\frac{1-\gamma^2}{\gamma^2}\left(\frac{1}{2\gamma}\ln\left(\frac{1+\gamma}{1-\gamma}\right)-1\right)}{2} \tag{4.5}$$

Where $\gamma = 1-(b/a)^2$

a and b are the semimajor and semiminor axis of an ellipsoid, respectively. Zeman and Schatz, generalized the effective depolarization factor to ellipsoids of revolution as

$$q_{eff} = q_b - \left(\frac{1}{3}\right)k^2b^2 - \left(\frac{2}{9}\right)ik^3b^3 \tag{4.6}$$

The effective screening factor (k_{eff}) for the dynamic Maxwell Garnett is based on the effective depolarization relation as follows,

$$k_{eff} = \left(\frac{1}{q_{eff}}\right)-1 \tag{4.7}$$

The effect of the size is reflected on the Maxwell Garnett relation on considering the effective screening factor (k_{eff}) (David E. Aspnes, 1982) in place of numeric value '2' under the equation 8, results as

$$\frac{\varepsilon_{MG} - \varepsilon_h}{\varepsilon_{MG} + k_{eff}\varepsilon_h} = f_a \frac{\varepsilon_a - \varepsilon_h}{\varepsilon_a + k_{eff}\varepsilon_h} + f_b \frac{\varepsilon_b - \varepsilon_h}{\varepsilon_b + k_{eff}\varepsilon_h} \quad (4.8)$$

The complex refractive index of the corresponding effective permittivity explicitly addresses the shape effect. This complex effective permittivity is then substituted in the scattering matrix computational technique where Maxwell's equation relates as,

$\nabla \times \vec{H} = k_0 \varepsilon_r \vec{E}$ under normalized magnetic field. The term, $k_0 = \frac{2\pi}{\lambda_0}$ is the free space wave number, where λ_0 is the free space wavelength. Hence, obtain the intensity of the transmitted light considering the dispersive property of the material.

From the figure 4.5, it is observed that with the increase in the aspect ratio of the prolate spheroid, the transmission dip reduces gradually within the wavelength range of 330nm-380nm. There is no significant change in the transmissivity along the visible light range with the change in shape of metal nanoparticles. Therefore it is better to have aspect ratio of the prolate spheroid close to value 'one' for minimum transmission within the UV-A range of spectrum,

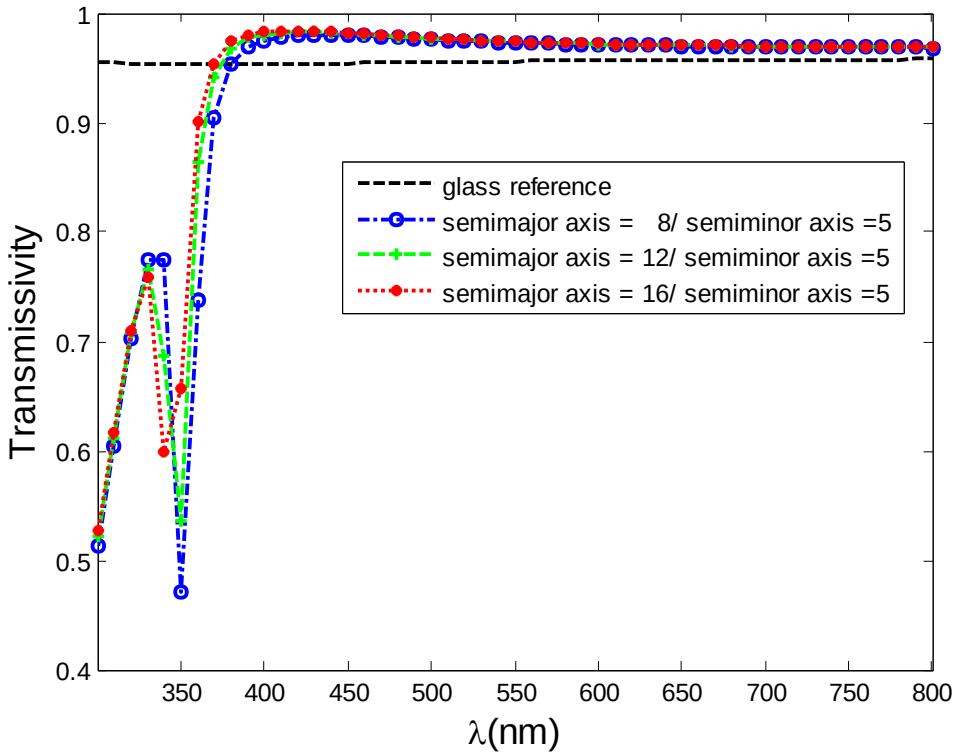

Figure 4.5. Effect of transmissivity with the change of the aspect ratio of silver nanoparticles prolate spheroid

In the proposed double layer thin film arrangement the metal(Silver) nanoparticles are embedded in the top layer. If the silver nanoparticles are embedded in the bottom instead of the top layer there seems to be a change in absorption spectrum in the near UV range. As seen from the figure 4.6, there is a marginal difference in the width of the absorption spectrum in the range of UV spectrum. However, the transmission dip is quite significant if the silver nanoparticles are placed in the lower layers of the thin film with slight deficit in the antireflection property in the visible light spectrum. Nevertheless, the silver nanoparticles possess the property of the plasmon

resonance irrespective of the layers to be considered for embedding the metal nanoparticles. The size of silver nanoparticles is considered to be 10nm.

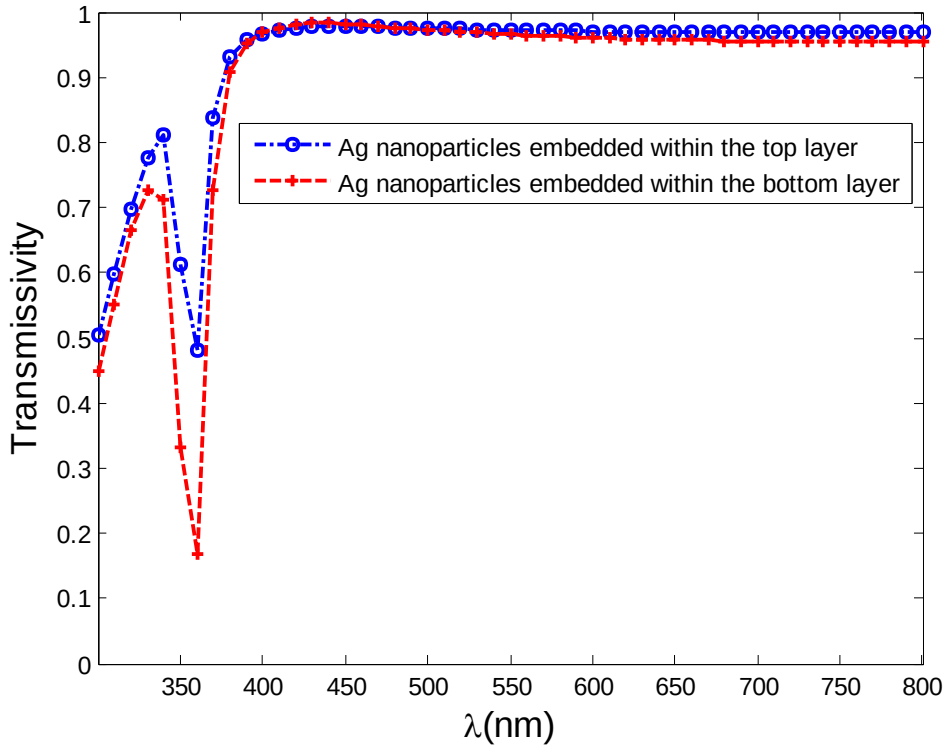

Figure 4.6. Effect of transmissivity with the alteration of the Silver nanoparticles inclusion in the two different layers of the double layer ARC coating.

Size Effect of TiO2 Inclusion:

The size effect of TiO2 inclusion on the light transmissivity across the proposed thin film structure is summarized in Table1. With the increase in the size of the TiO2 inclusion while considering fixed size of 10nm Silver inclusion in the thin film arrangement, there is deterioration in the transmissivity of light under the visible spectrum. On comparing the different sizes of the TiO2 nanoparticle inclusions in the

host medium it is observed that the transmissivity of light across the thin film structure gradually decreases, irrespective of the two ranges of wavelength, split between near UV

Table1 : Effect of transmissivity on size variation of TiO2 nanoparticles on both layers of ARC

Transmissivity of UV protected Anti-Reflection Coating			
Range of Wavelength	Size of TiO2 inclusion in the thin film arrangement		
	10nm	30nm	40nm
300nm-400nm	0.7325	0.5379	0.3328
400nm-800nm	0.9704	0.9454	0.9052

light and visible light spectrum. Drop in the transmissivity within the range of UV spectrum is beneficial but have to compromise with the lowering of antireflection properties in the range of visible light spectrum. Hence it is evident that the sizes of both the inclusions i.e., Ag nanoparticles and TiO2 nanoparticles need to be small (in the order of 10nm) to achieve anti-reflection property with partial ultraviolet block in the range of near-UV.

On considering the TiO2 nanoparticles size variation under the lower layer with the upper layer TiO2 nanoparticles size constant (10nm) the effect of transmission is observed in Table2. Until now, we have considered the size variation of nanoparticles on both the layers of thin film arrangement. However, on considering the variation of inclusion size within lower layer does not reflect significant deviation from the change in

Table2 : Comparison of transmissivity between the different TiO2 nanoparticles size based ARC

Transmissivity of ARC over the near UV and Visible light spectrum				
Size of TiO2 inclusion	Range of light Wavelength			
	300nm-400nm		400nm-800nm	
	TiO2 in both layers of ARC	TiO2 in lower layer (TiO2 in upper layer is fixed,10nm)	TiO2 in both layers of ACR	TiO2 in lower layer (TiO2 in upper layer is fixed,10nm)
10nm	0.7325	0.7326	0.9704	0.9706
30nm	0.5379	0.5995	0.9454	0.9561
40nm	0.3328	0.4341	0.9052	0.9323

both the layers. As the size of the TiO2 inclusion increases under the lower layer the transmissivity decrease along the lower wavelength range of visible spectrum(300nm-450nm).

Scattering of Light:

The scattered irradiance per unit incident irradiance is given by following relations :

$$i_{\parallel} = S_{11} + S_{12} = Q_{11} + Q_{12}$$
$$i_{\perp} = S_{11} - S_{12} = Q_{22} + Q_{12} \qquad (4.9)$$

Where

$i_{\parallel}$ is the scattered irradiance for incident light parallel to the scattering plane.

$i_{\perp}$ is the scattered irradiance for incident light perpendicular to the scattering plane.

Considering the above relation the incident unpolarized light is

$$i = \frac{i_{\parallel} + i_{\perp}}{2} = S_{11} \tag{4.10}$$

Where, S_{11} is the dimensionless scattered irradiance.

If unpolarized light is incident over a surface then the scattered light will sustain a degree of linear polarization stated as

$$P = -\frac{S_{12}}{S_{11}} = \frac{Q_{22} - Q_{11}}{Q_{11} + 2Q_{12} + Q_{22}} \tag{4.11}$$

And cross polarization, $Q_{11} = \frac{1}{2}\left(S_{11} - S_{22}\right)$ (4.12)

Under the spherical shape of a particle the cross polarization does not exist and the following relation holds:

$$P = \frac{Q_{22} - Q_{11}}{Q_{11} + Q_{22}}, i_{\parallel} = Q_{11}, i_{\perp} = Q_{22} \tag{4.13}$$

The relationship between the following parameters stated below,

$I_s(\theta,\phi)$, scattered irradiance

I_i, the incident irradiance

and the distance ‘r’ to the detector

will define the differential scattering cross-section $dC_{sca} / d\Omega$

as $$\frac{dC_{sca}}{d\Omega} = \frac{r^2 I_s}{I_i} \tag{4.14}$$

The differential scattering cross-section is the energy scattered per unit time into a unit solid angle. The scattering angle θ and the azimuthal angle ϕ will direct the scattered light towards a specific angle.

For unpolarized incident light the differential scattering cross-section is represented as

$$\frac{dC_{sca}}{d\Omega} = \frac{S_{11}}{K^2} = \frac{i_{11} + i_{\perp}}{2K^2} \tag{4.15}$$

For an isotropic medium such as collection of many randomly oriented particles, the scattered irradiance and hence the differential scattering cross section is independent of ϕ ,(Azumuthal angle).

For small size parameters, the familiar Rayleigh scattering pattern are obtained: perpendicularly polarized light is scattered isotropically, while light polarized parallel to the scattering planes vanishes at a scattering angle of 90^0 ; as a consequence, incident unpolarized light is completely polarized at 90^0.

The normalized matrix element S_{22} / S_{11} , which is unity for all spheres. The departure of S_{22} / S_{11} from unity is a measure of non-sphericity; the difference $\Delta = 1 - S_{22} / S_{11}$ is also called the depolarization ratio. If Δ is zero, there is no depolarization of incident light polarized either parallel on perpendicular to the scattering

plane. Nonspherical particles will be partially oriented if they are in a flow system or if they are subjected to electric or magnetic fields. Such partial orientations influence the light scattering.

An approximate formula of transmission coefficient for a given thin film layer is expressed as

$T = \frac{1}{(1+X)^2}$ where X is represented in the form as follows

For s-polarized light,

$$X_s = \frac{1}{n_0 \cos\theta_0 + n_2 \cos\theta_2} \frac{2\pi d}{\lambda} \Im\varepsilon \tag{4.16}$$

For p-polarized light,

$$X_p = \frac{1}{(\cos\theta_0 / n_0) + (\cos\theta_2 / n_2)} \frac{2\pi d}{\lambda} \left\{ \frac{\cos\theta_0 \cos\theta_2}{n_0 n_2} \Im\varepsilon + {n_0}^2 \sin^2\theta_0 \Im\frac{1}{\varepsilon} \right\} \tag{4.17}$$

Here is the complex dielectric constant of the film substrate, d the film thickness, λ the wavelength of light in vacuum, θ_0 the angle of incidence from the medium of index and θ_2 the angle of refraction into the medium of index n_2. Under the condition where $n_0 = n_2$, the terms in X_s and X_p represent the absorption due to the polarization induced by the component of applied electric field parallel to the thin film and the terms in X_p expresses the absorption due to the polarization induced by the component of that field normal to the film. The optical absorption in a substance occurs in proportion to $\Im\varepsilon$, ε being the complex dielectric constant of the substance, while the fast electrons lose their kinetic energy by $\hbar\omega$. The optical absorption of thin film made of silver is different

from that of the thick homogeneous slab or that for bulk silver (Meyer et al., 1967) (Yamaguchi, 1962).

As seen from the figure 4.7 it is observed that with the decrease in the elevation angle the transmissivity reduces along the visible light spectra. This results in the deterioration of antireflective property. However, the UV blocking property along the near ultraviolet region is not affected with the change in the angle of incident. It is preferred to have normal incidence of light for maximum transmission and minimum reflection.

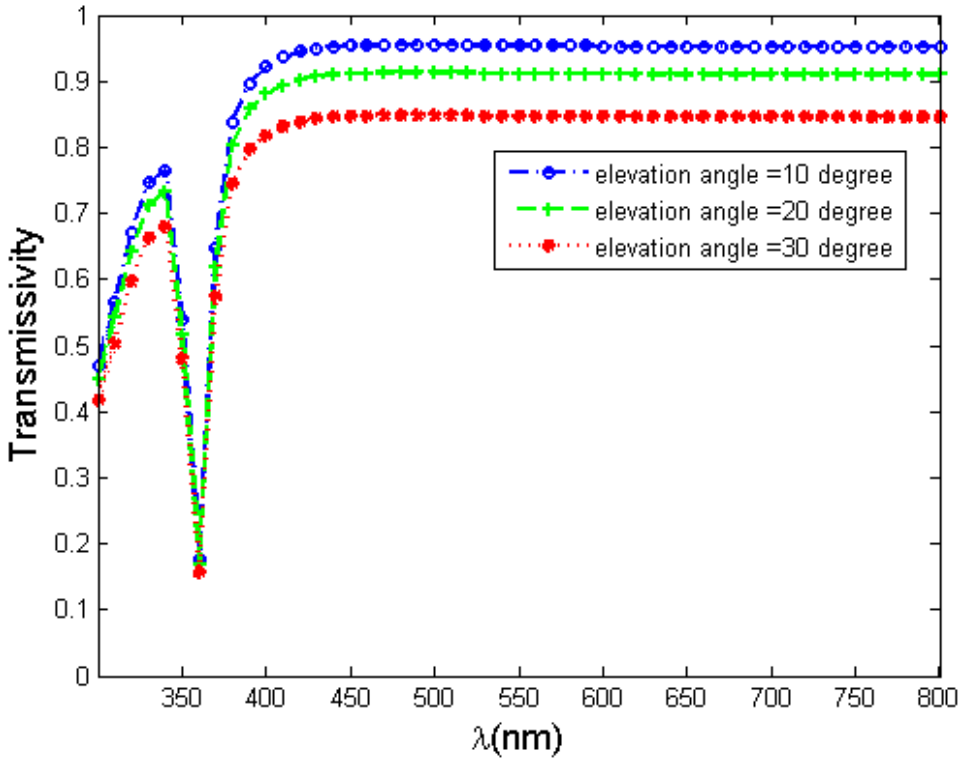

Figure 4.7. Effect of transmissivity with the change in the elevation angle of the incident light on the ARC.

A comparative study is conducted over a range of specific metals nanoparticles to understand its effects of absorption in the ultraviolet range of light spectrum. Here, the specific metals are considered which inherits the quality of localize surface plasmons. Among them the major metal nanoparticles tends to absorb in the range of UV-B and UV-C. The Gold and Silver are the only two metals which are inclined towards the absorption of light in the range of near UV and visible spectrum. The peak absorption in the range of near UV spectrum is prominent in the silver metal nanoparticles as shown in figure 4.8.

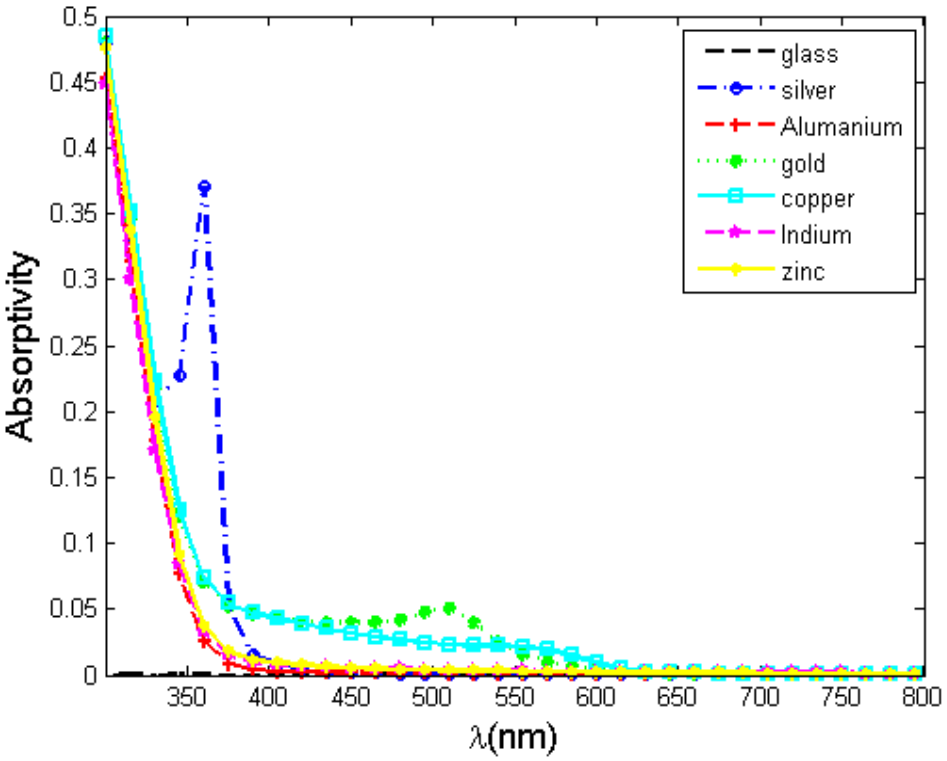

Figure 4.8. Absorptivity of the ARC under various nano-particle metals as inclusion.

Thin Film Deposition Method

There exist various deposition technologies to grow thin films used as optical components, electronic devices and magnetic sensors. Various techniques are adopted to deposit thin film over the substrate such as chemical vapor deposition (CVD), physical vapor deposition (PVD), liquid-phase processes, and writing/printing methods. The following deposition technique is considered feasible to obtain the desired thin film for our application.

1. Pulse Laser Deposit for thin film

The complex oxide thin films are normally developed by pulse laser deposition(PLD) technique. The PLD technique is a physical vapor deposition process. The formulation of complex oxide nanostructure can be achieved using the PLD technique where a solid material can stoichiometrically transfer to a thin film substrate. The drawbacks in the thin film produced by PLD technique is the uniformity issue under broad surface. This is because of narrow forward angular distribution of plasma plume from the target material. Along with the following advantages we need to analyze the drawback of the mentioned deposition technique.

The prominent disadvantage of PLD technique is the generation of rough surface with uneven uniformity. This is caused because of the narrow forward angular distribution of the plasma plume which emits from the target gun. Another effect termed as the surface boiling is observed during fabrication which leads to the surface defeat and random spot particulate concentration. Considering surface augmentation with large particulates size (in the range of micrometer) is a challenge as this will seriously influence the surface

texturization. This characteristic also alters the electrical properties of the films and prevents the growth of thin film in industrial-scale. Latest innovative methods under deposition technique, such as rotating both target and substrate and using a shadow mask to obstruct the flow of particulates in order to fabricate a large and uniform film, have been developed to improve the film quality.

2. Electron Beam Evaporation Deposition

The advancement in surface-sensitivity probes, vacuum technology and electron diffraction technique has contributed a lot in control growth of thin films. The development of vacuum technology reduces surface contamination and contamination while growing thin film. Electron beam deposition uses electrons to evaporate the materials which will deposited over the substrate in the form of thin film. This method eliminates the contamination by crucibles, heaters, and support materials. This method is good for the fabrication of highly pure film. Au, Ag and TiO2 can be evaporated by an electron beam as power densities in the range of 100 W/cm2 can be reached in a smaller area. In order to maintain the purity of the thin film the source material is placed in the water-cooling crucible, which can avoid contamination from the evaporation of the material of the container, and the reaction between the material of the container and the coating material, which is crucial for improving the purity of the thin film that is coating on the substrate.

3. Thin Film Deposition using Sputtering

Nanomaterials can also be fabricated as thin film using one of the important physical vapor deposition (PVD) techniques termed as sputtering technique. This

sputtering process involves the physical vaporization of atoms from a surface by energetic ions accelerating towards the target. Sputtering technologies can be applied for the growth of thin films with different surface structure of metal and compound depositions. Fabrication of functional nanowires, nanobelts and thin films by magnetic sputtering is possible. Metal alloy thin films and Composite metal oxide thin films are the recently developed nanomaterials that can be fabricated using the sputtering technique. Molecular beam epitaxy (MBE) growth technology is one of several methods to deposit single crystals. MBE offers a precise control regulation over film thickness however the growth rate is sufficiently slow. MBE growth is normally used in nanostructures based on oxide and III–V semiconductors.

4. Thin film deposition using Atomic Layer Deposition

Atomic layer deposition (ALD) is one of the best nanofilm deposition methods as one can achieve high aspect nanostructure. Precise thickness control in the scale on nanometer can be achieved using ALD. The group of M. Leskela in the year 2014 has grown Nanolaminate of TiO2 and Ho2O3 on Si (001) substrates by ALD. TiO2 nanofilm was designed by Dr Buchalska using ALD, where the TiO2 was deposited on the native oxide covered Si (100). The property of conformal coating in ALD process helps in the reduction of pore size over the Nanoporous surfaces. This regulation of the free space volume in a porous material can change the optical and electrical property.

4.3 Findings of the Study

Three-Layer ARC

With the increase in the numbers of thin film layers to three, the broadening of the transmission maxima along the visible light spectrum is more prominent as compared to the double layer ARC.

On considering the three layers, by giving it a finite thickness we can further reduce the residual reflectance to enhance the AR properties and increase the bandwidth. The actual amount of the thickness depends on the phase factor and is difficult to optimize. Hence, based on the reflective index relation, $\eta_2 / \eta_1 = \eta_3 / (\eta_M \eta_S)^{1/2}$ the optimal bandwidth should be determined by varying the refractive index of any two layers from the three layer coating as the value of the refractive index of the substrate(η_S) is 1.52 and the air medium(η_M) is known under a specific wavelength(500nm) as the material is considered as dispersive medium. The refractive of the middle layer(η_2) is considered to be 1.63 henceforth, the top layer is 1.3(η_1) and the bottom layer(η_3) is 1.5.

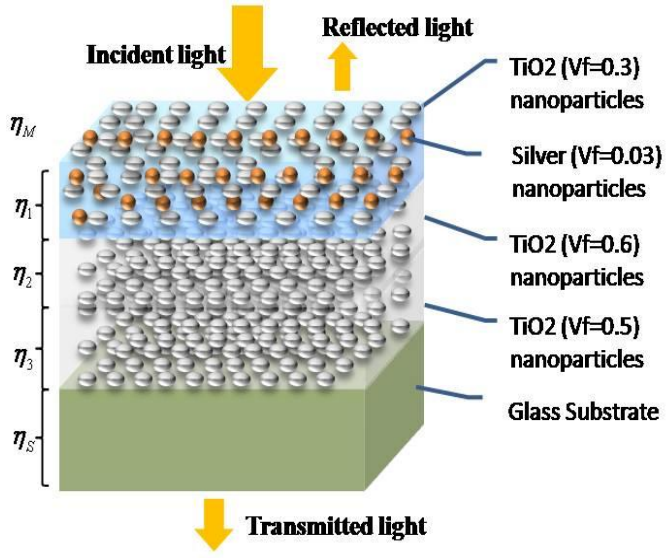

Figure 4.9. Schematic view of the triple layer ARC

For the corresponding layers thickness should be 500nm/(η_1 x4) i.e 96nm for the top layer, 500nm/(η_1 x2) i.e 153nm for the middle layer and 500nm/(η_1 x2) i.e 167nm for the bottom layer.

Based on the figure 4.10 it is evident that the nanoparticles embedded on the bottom layer give greater obstruction to ultra violet radiation as compared to the metal nanoparticles embedded on the top layer. As compared to the double layer arrangement the three layer thin film coating give better transmission within the range of visible light

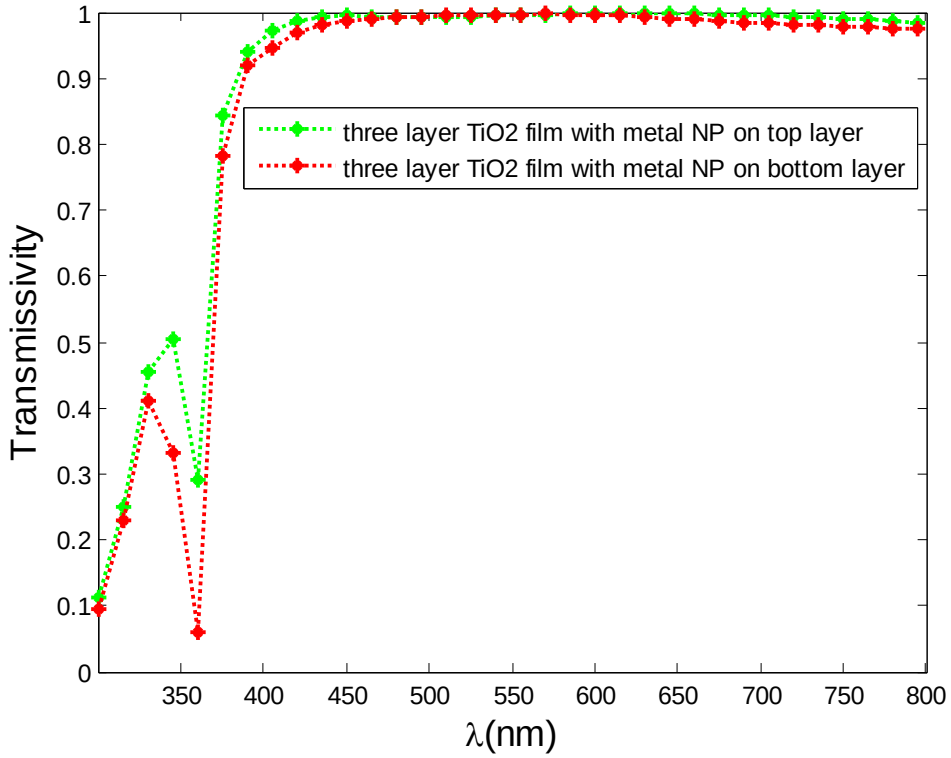

Figure 4.10. Comparative study on the effect of transmissivity between metal nanoparticles on the top layer of three layers ARC and bottom layer of three layers ARC.

spectrum. Moreover, the three layer antireflection coating has near UV light blocking property at par with the double layer antireflection coating. Nevertheless, we have to comprise with the complexity of triple layer fabrication for an enhanced antireflection coating with an average of two percentage increase in the transmissivity within the range of visible light spectrum.

On considering the Silver nanoparticle embedded in the top layer leads to better transmissivity which is not appreciable under our application. However, the transmissivity under the range between 400nm to 8000nm is better compared to the metal

Table3. Comparison of transmissivity between different locations of Silver nanoparticles in ARC layers

Transmissivity of ARC over the near UV and Visible light spectrum		
Allocation of metal nanoparticles	Range of light Wavelength	
	300nm-400nm	400nm-800nm
Top Layer	0.5280	0.9931
Bottom Layer	0.4489	0.9864

nanoparticles embedded in the bottom layer as shown in table3. Thus, it is justified to embed the silver nanoparticles within the bottom layer which would result in higher degree of UV blocking with marginal loss of antireflection property in the visible light spectrum as compared to the silver nanoparticle in the top layer.

4.4 Conclusion

The above result suggests an arrangement of thin films design to act as an antireflection coating in the range of visible light spectrum which have the property of partial blocking the UV radiation(in the range of 320nm-370nm) and high frequency blue light radiation. With the metal nanoparticles embedded in the thin film layer it is possible to design antireflection coating with the property of near UV blocking. Regulating the shape and size of the nanoparticles would lead to the shifting of transmission dip within the range of ultra violet radiation. On considering two layers of porous thin film based on W-type coating with the top layer consisting of TiO2 and silver inclusion and bottom layer of TiO2, an efficient antireflection property can be achieved. Finally, the transmitted spectrum characteristic can be tuned by manipulating the volume fraction of the inclusions in the host, size and shape of the metal nanoparticles inclusion and thickness of the thin film layer arrangement.

CHAPTER 5

DISCUSSION

5.1 Hypotheses Summary

It is often desired to have multilayer thin film coating with appropriate index of refraction to achieve effective anti-reflection properties. However, it is rare to extract material with specific refractive index in nature. Therefore, an effective medium has to be devised for the required dielectric constant. An ARC structure is proposed which will consist of metal NPs in thin film structures, which have localized surface plasmon resonance properties. These metal NPs will block the near-UV light while simultaneously exhibiting ultralow reflectivity in the visible light range by regulating its concentration and size.

5.2 Discussion

It has been observed that with the increase in the size of the Silver nanoparticles the amount of transmission dip reduces in the blue light region which hampers the blocking capacity. Hence it is recommended to constrict the size of nanoparticles within the 10nm radius. Furthermore, with the change in the aspect ratio of the prolate nano-spheroid the transmission of light gets effect under the near UV range. Low aspect ratio of the nano-spheroid results in the increase of the absorption of light within the thin film which in turn impedes transmission of UV light through the thin film ARC.

The double layer antireflection coating is designed based on w-type coating for broader reflection minimum throughout the range of visible light spectrum. Considering the required refractive index of the material for the effective antireflection property the volume fraction of TiO2 has been tuned to 0.3 for the upper layer and 0.5 for the lower layers in air as the host medium. On embedding Silver nanoparticles in the lower layer of the double layer thin film arrangement leads to better performance in blocking near UV region then on embedding on the upper layer.

Increase in the size of the TiO2 inclusion leads to wide spectrum of UV blocking compromising the antireflective properties under the visible light spectrum. Hence it is preferred to have TiO2 inclusion size within the range of 10nm in the air host medium. On comparing, the TiO2 size variation in the lower layers with respect to TiO2 size variation on both the layer leads to marginal difference in the transmission effect. Finally it is preferred to have double layer thin film based w-type coating with TiO2 particles size of less than 10nm and the silver nanoparticles embedded in the upper layers with size of around less than 10nm.

5.3 Recommendation for Further Application

Thin film coating is critical for optical coating applications. The growth in the field of optical data storage devices such as computer memory and storage disk necessitates the rise in the need for the development of advance thin film coating. The thin film arrangement acts as a coating shield to prevent the substrate for direct atmospheric degradation and protect against temperature rise. It can be used in coating

glass structure and mirror to prevent heat or ultra violet radiation from passing through. It can also filter greater amount of light into the photovoltaic cell to enhance the number of electrons and holes generation. AR coating with appropriate refractive index gradient can improve refraction and absorption coefficient performance on optical fibers. For the laser optics application, subject has to endure enormously high radiation without considerable degradation. This can be achieved by highly reflective thin film coating over the subject devised as antireflection coating. The coating which would reflect infrared radiation can be applicable to increase the luminous flux intensity of a filament.

More methodological work is needed to fabricate a robust and efficient ARC with lower disintegrating rate. Different deposition techniques has to be analyzed for surface modification and coating. The impact of surface layered metal and dielectric nanoparticles has not been captured. In-depth exploration of how broader reflectance minimum can be achieved with lesser number of thin film layers is required.

BIBLIOGRAPHY

Abhandlungen über die mechanische Wärmetheorie. by Clausius, R.: 8°, HLdrbde. der Zeit. (1864) | *Antiquariat und Café Antiquarius.* Retrieved October 30, 2020, from https://www.abebooks.co.uk/Abhandlungen-mechanische-W%C3%A4rmetheorie-Clausius-R-Braunschweig/3057887786/bd

Ag-assisted electrochemical etching of silicon for antireflection in large area crystalline thin film photovoltaics—IEEE Conference Publication. Retrieved October 23, 2020, from https://ieeexplore.ieee.org/abstract/document/6318118

Andrews, D., Scholes, G., & Wiederrecht, G. (2010). *Comprehensive nanoscience and technology*. Academic Press.

Anti-reflective coatings: A critical, in-depth review—Energy & Environmental Science (RSC Publishing). Retrieved October 11, 2020, from https://pubs.rsc.org/en/content/articlelanding/2011/ee/c1ee01297e#!divAbstract

Aspnes, D. E. (1982a). *Optical properties of thin films. Thin Solid Films, 89*(3), 249–262. https://doi.org/10.1016/0040-6090(82)90590-9

Aspnes, D. E. (1982b). *Optical properties of thin films. Thin Solid Films, 89(3)*, 249–262. https://doi.org/10.1016/0040-6090(82)90590-9

Aspnes, D. E. (1982). *Optical properties of thin films. Thin Solid Films, 89(3)*, 249–262.

Austin, R. R. (1992). *Multilayer anti-reflection coating using zinc oxide to provide ultraviolet blocking. Google Patents.*

Berreman, D. W. (1963). *Infrared absorption at longitudinal optic frequency in cubic crystal films. Physical Review, 130(6), 2193.*

Bilyalov, R. R., Lüdemann, R., Wettling, W., Stalmans, L., Poortmans, J., Nijs, J., Schirone, L., Sotgiu, G., Strehlke, S., & Lévy-Clément, C. (2000). *Multicrystalline silicon solar cells with porous silicon emitter. Solar Energy Materials and Solar Cells, 60*(4), 391–420.

Bird, R. B. (1964). *The Feynman lectures on physics, Richard P. Feynman, Robert B. Leighton, and Matthew Sands, Addison-Wesley, Reading, Mass, Volume I, II (1964); Volume III (1965). AIChE Journal, 10*(6), 794–794. https://doi.org/10.1002/aic.690100602

Bisegna, F., Borra, M., Leccese, F., & Asdrubali, F. (2018). *Prevention of UV Radiation Hazard. 2018 IEEE International Conference on Environment and Electrical Engineering and 2018 IEEE Industrial and Commercial Power Systems Europe (EEEIC / I CPS Europe)*, 1–6. https://doi.org/10.1109/EEEIC.2018.8494519

Blue light hazard and aniridia. | British Journal of Ophthalmology. Retrieved October 12, 2020, from https://bjo.bmj.com/content/69/3/233.short

Bohren, C. F. (1986). *Applicability of effective-medium theories to problems of scattering and absorption by nonhomogeneous atmospheric particles. Journal of the Atmospheric Sciences, 43*(5), 468–475.

Bohren, C. F., & Huffman, D. R. (2008). *Absorption and scattering of light by small particles. John Wiley & Sons.*

Brückner, C., Pradarutti, B., Stenzel, O., Steinkopf, R., Riehemann, S., Notni, G., & Tünnermann, A. (2007). *Broadband antireflective surface-relief structure for THz optics. Optics Express, 15*(3), 779–789.

Bullough, J. D. (2000). *The Blue-Light Hazard: A Review. Journal of the Illuminating Engineering Society*, *29*(2), 6–14. https://doi.org/10.1080/00994480.2000.10748312

Characterization and properties of a textured silicon surface with nano-porous layer—IEEE Conference Publication. Retrieved October 23, 2020, from https://ieeexplore.ieee.org/abstract/document/4388801

Cid, M., Stem, N., Brunetti, C., Beloto, A. F., & Ramos, C. A. S. (1998). *Improvements in anti-reflection coatings for high-efficiency silicon solar cells. Surface and Coatings Technology*, *106*(2), 117–120. https://doi.org/10.1016/S0257-8972(98)00499-X

Cross, G. H. (2013). *Fundamental limit to the use of effective medium theories in optics. Optics Letters, 38*(16), 3057–3060.

Derkacs, D., Lim, S. H., Matheu, P., Mar, W., & Yu, E. T. (2006). *Improved performance of amorphous silicon solar cells via scattering from surface plasmon polaritons in nearby metallic nanoparticles. Applied Physics Letters, 89*(9), 093103.

Ferry, V. E., Munday, J. N., & Atwater, H. A. (2010). *Design considerations for plasmonic photovoltaics. Advanced Materials, 22*(43), 4794–4808.

Feuillade, M., & Maury, H. (2020). *Ophthalmic Lens Comprising a Multilayered Interferential Coating and Manufacturing Method Thereof (United States Patent*

No. US20200041697A1).

https://patents.google.com/patent/US20200041697A1/en

Fleischmann, M., Hendra, P. J., & McQuillan, A. J. (1974). *Raman spectra of pyridine adsorbed at a silver electrode. Chemical Physics Letters, 26*(2), 163–166.

Fraunhofer, J. (1888). *Joseph von Fraunhofer Gesannekte Schri 鎔 en.* Munich, Germany.

Garnett, J. M. (1904). XII. *Colours in metal glasses and in metallic films. Philosophical Transactions of the Royal Society of London. Series A, Containing Papers of a Mathematical or Physical Character, 203*(359–371), 385–420.

Giovanetti, A. (2015). *Cerium oxide nanoparticles, combining antioxidant and UV shielding properties, prevent UV-induced cell damage and mutagenesis.*

Gombert, A., Rose, K., Heinzel, A., Horbelt, W., Zanke, C., Bläsi, B., & Wittwer, V. (1998). *Antireflective submicrometer surface-relief gratings for solar applications. Solar Energy Materials and Solar Cells, 54*(1), 333–342. https://doi.org/10.1016/S0927-0248(98)00084-1

Gottwald, A., Wiese, K., Siefke, T., & Richter, M. (2019). *Validation of thin film TiO2 optical constants by reflectometry and ellipsometry in the VUV spectral range. Measurement Science and Technology, 30*(4), 045201.

Ham, W. T., Mueller, H. A., & Sliney, D. H. (1976). *Retinal sensitivity to damage from short wavelength light. Nature, 260*(5547), 153–155. https://doi.org/10.1038/260153a0

Heller, W. (1965). *Theoretical investigations on the light scattering of spheres. XVI. Range of practical validity of the Rayleigh theory. The Journal of Chemical Physics, 42*(5), 1609–1615.

Hornyak, G. L., Patrissi, C. J., & Martin, C. R. (1997). *Fabrication, characterization, and optical properties of gold nanoparticle/porous alumina composites: The nonscattering Maxwell- Garnett limit. The Journal of Physical Chemistry B, 101*(9), 1548–1555.

Improved porous silicon-based multifunctional materials for the solar cells antireflection coating—IEEE Conference Publication. Retrieved October 23, 2020, from https://ieeexplore.ieee.org/abstract/document/7500990/

International Commission on Non-Ionizing Radiation Protection. (2010). ICNIRP statement—*Protection of workers against ultraviolet radiation. Health Physics, 99(*1), 66–87. https://doi.org/10.1097/HP.0b013e3181d85908

Jenkins, P., Landis, G. A., Fatemi, N., Li, X., Scheiman, D., & Bailey, S. (1992). *Increased efficiency with surface texturing in ITO/InP solar cells. LEOS 1992 Summer Topical Meeting Digest on Broadband Analog and Digital Optoelectronics, Optical Multiple Access Networks, Integrated Optoelectronics, and Smart Pixels, 186–189.* https://doi.org/10.1109/ICIPRM.1992.235646

Karlsson, M., & Nikolajeff, F. (2003). *Diamond micro-optics: Microlenses and antireflection structured surfaces for the infrared spectral region. Optics Express, 11*(5), 502–507. https://doi.org/10.1364/OE.11.000502

Karmakar, B. (2017). *Functional Glasses and Glass-Ceramics: Processing, Properties and Applications. Butterworth-Heinemann.*

Kats, M. A., Blanchard, R., Genevet, P., & Capasso, F. (2013). *Nanometre optical coatings based on strong interference effects in highly absorbing media. Nature Materials, 12*(1), 20–24.

Kats, M. A., Sharma, D., Lin, J., Genevet, P., Blanchard, R., Yang, Z., Qazilbash, M. M., Basov, D. N., Ramanathan, S., & Capasso, F. (2012). *Ultra-thin perfect absorber employing a tunable phase change material. Applied Physics Letters, 101*(22), 221101.

Kim, S.-S., Na, S.-I., Jo, J., Kim, D.-Y., & Nah, Y.-C. (2008). *Plasmon enhanced performance of organic solar cells using electrodeposited Ag nanoparticles. Applied Physics Letters, 93*(7), 305.

Kneipp, K., Moskovits, M., & Kneipp, H. (2006). *Surface-Enhanced Raman Scattering: Physics and Applications. Springer Science & Business Media.*

Koledintseva, M. Y., DuBroff, R. E., & Schwartz, R. W. (2006). *Maxwell Garnett Model for Dielectric Mixtures Containing Conducting Particles at Optical Frequencies.* Missouri Univ-Rolla.

Kumari, M., Ding, B., & Blaikie, R. (2016). *Enhanced resonant absorption in dye-doped polymer thin-film cavities for water vapour sensing. Sensors and Actuators B: Chemical, 231*, 88–94.

Lee, E., & Lee, S. (2006). *Characterization and properties of a textured silicon surface with nano-porous layer. 2006 IEEE Nanotechnology Materials and Devices Conference, 1,* 430–431.

Lérondel, G., Romestain, R., & Barret, S. (1997). *Roughness of the porous silicon dissolution interface. Journal of Applied Physics, 81*(9), 6171–6178.

Li, L. (1996). *Formulation and comparison of two recursive matrix algorithms for modeling layered diffraction gratings. JOSA A, 13*(5), 1024–1035.

Li, X. (2012). *Metal assisted chemical etching for high aspect ratio nanostructures: A review of characteristics and applications in photovoltaics. Current Opinion in Solid State and Materials Science, 16*(2), 71–81. https://doi.org/10.1016/j.cossms.2011.11.002

Lu, C., & Liu, C. W. (2015). *Antireflection of nano-sized SiO sphere arrays on crystalline silicon solar cells. 2015 International Conference on Numerical Simulation of Optoelectronic Devices (NUSOD), 145–146.* https://doi.org/10.1109/NUSOD.2015.7292864

Macleod, H. A. (1986). *Thin-Film Optical Filters Hilger.* Bristol, UK, 19862, 148.

Markel, V. A. (2016a). *Introduction to the Maxwell Garnett approximation: Tutorial. JOSA A, 33*(7), 1244–1256.

Markel, V. A. (2016b). *Maxwell Garnett approximation (advanced topics): Tutorial. JOSA A, 33*(11), 2237–2255.

Markel, V. A. (2016c). *Introduction to the Maxwell Garnett approximation: Tutorial. JOSA A, 33*(7), 1244–1256. https://doi.org/10.1364/JOSAA.33.001244

Meyer, E., Frede, H., & Knof, H. (1967). *Optical Effects in Metals: Application of a Least-Squares Method to Measurements on Gold and Silver. Journal of Applied Physics, 38*(9), 3682–3684. https://doi.org/10.1063/1.1710194

Mittleman, D. M. (2005). *Imaging and Sensing with Terahertz Radiation. AIP Conference Proceedings, 760*(1), 25–32. https://doi.org/10.1063/1.1916656

Mossotti, O. F. (1846). *Discussione analitica sull'influenza che l'azione di un mezzo dielettrico ha sulla distribuzione dell'elettricità alla superficie di più corpi elettrici disseminati in esso. dai tipi della r. D. camera.*

Motamedi, M. E., Southwell, W. H., & Gunning, W. J. (1992). *Antireflection surfaces in silicon using binary optics technology. Applied Optics, 31*(22), 4371–4376.

Musset, A., & Thelen, A. (1970). *IV multilayer antireflection coatings. In Progress in optics (Vol. 8, pp. 201–237). Elsevier.*

Nakayama, K., Tanabe, K., & Atwater, H. A. (2008). *Plasmonic nanoparticle enhanced light absorption in GaAs solar cells. Applied Physics Letters, 93*(12), 121904.

Nishioka, K., Sueto, T., & Saito, N. (2009). *Formation of antireflection nanostructure for silicon solar cells using catalysis of single nano-sized silver particle. Applied Surface Science, 255*(23), 9504–9507.

Optical analysis of textured surfaces for photovoltaic solar cells—IEEE Conference Publication. Retrieved October 23, 2020, from https://ieeexplore.ieee.org/abstract/document/161812

Opticks: Or, a Treatise of the Reflections, Refractions, Inflections and Colours of Light. The Second Edition, with Additions | Isaac NEWTON. Retrieved October 12,

2020, from https://www.jonathanahill.com/pages/books/3019/isaac-newton/opticks-or-a-treatise-of-the-reflections-refractions-inflections-and-colours-of-light-the-second

Oyama, T., Ohsaki, H., Tachibana, Y., Hayashi, Y., Ono, Y., & Horie, N. (1999). *A new layer system of anti-reflective coating for cathode ray tubes. Thin Solid Films, 351*(1–2), 235–240.

Palik, E. D. (1998). *Handbook of Optical Constants of Solids. Academic Press.*

Physics 435—*Prof. S. Errede's Lecture Notes—Fall Semester, 2007.* Retrieved October 23, 2020, from http://web.hep.uiuc.edu/home/serrede/P435/P435_Lectures.html

Pillai, S., Catchpole, K. R., Trupke, T., & Green, M. A. (2007). *Surface plasmon enhanced silicon solar cells. Journal of Applied Physics, 101*(9), 093105.

Porous silicon in crystalline silicon solar cells: A review and the effect on the internal quantum efficiency—Stalmans—1998—Progress in Photovoltaics: Research and Applications—Wiley Online Library. Retrieved October 23, 2020, from https://onlinelibrary.wiley.com/doi/abs/10.1002/(SICI)1099-159X(199807/08)6:4%3C233::AID-PIP207%3E3.0.CO;2-D

Rayleigh, Lord. (1879). *On Reflection of Vibrations at the Confines of two Media between which the Transition is Gradual. Proceedings of the London Mathematical Society, s1-11*(1), 51–56. https://doi.org/10.1112/plms/s1-11.1.51

Rea, M. S. (2000). *The IESNA lighting handbook: Reference & application (9th ed.). Illuminating Engineering Society of North America.*

Redheffer, R. (1961). *Difference equations and functional equations in transmission-line theory. Modern Mathematics for the Engineer, 12,* 282–337.

Rensberg, J., Zhang, S., Zhou, Y., McLeod, A. S., Schwarz, C., Goldflam, M., Liu, M., Kerbusch, J., Nawrodt, R., & Ramanathan, S. (2016). *Active optical metasurfaces based on defect-engineered phase-transition materials. Nano Letters, 16*(2), 1050–1055.

Ru, E. L., & Etchegoin, P. (2008). *Principles of Surface-Enhanced Raman Spectroscopy: And Related Plasmonic Effects. Elsevier.*

Rumpf, R. C. (2011). *Improved formulation of scattering matrices for semi-analytical methods that is consistent with convention. Progress In Electromagnetics Research, 35,* 241–261.

Sarker, J. C., Makableh, Y. F., Vasan, R., Lee, S., Manasreh, M. O., & Benamara, M. (2016). *Broadband nanostructured antireflection coating for enhancing GaAs solar cell performance. IEEE Journal of Photovoltaics, 6*(6), 1509–1514.

Schlich, F. F., & Spolenak, R. (2013). *Strong interference in ultrathin semiconducting layers on a wide variety of substrate materials. Applied Physics Letters, 103*(21), 213112.

Schnell, M., Ludemann, R., & Schaefer, S. (2000). *Plasma surface texturization for multicrystalline silicon solar cells. Conference Record of the Twenty-Eighth IEEE Photovoltaic Specialists Conference-2000* (Cat. No. 00CH37036), 367–370.

Spinelli, P., Hebbink, M., De Waele, R., Black, L., Lenzmann, F., & Polman, A. (2011). *Optical impedance matching using coupled plasmonic nanoparticle arrays. Nano Letters, 11*(4), 1760–1765.

SR, H. J. A., Stephan, T. G., & Bernardi, A. (2016). *Visible spectrum anti-reflective coatings with reduced reflections in ultraviolet and infrared spectral bands (United States Patent No. US9291746B2).* https://patents.google.com/patent/US9291746B2/en

Taliercio, T., Guilengui, V. N., Cerutti, L., Tournié, E., & Greffet, J.-J. (2014). *Brewster "mode" in highly doped semiconductor layers: An all-optical technique to monitor doping concentration. Optics Express, 22*(20), 24294–24303.

Taylor, H. R. (1989). *The biological effects of UV-B on the eye. Photochemistry and Photobiology, 50*(4), 489–492.

Tian, Z.-Q., Yang, Z.-L., Ren, B., & Wu, D.-Y. (2006). *SERS from transition metals and excited by ultraviolet light. In Surface-Enhanced Raman Scattering (pp. 125–146). Springer.*

Ultraviolet eye damage: The epidemiological evidence. Retrieved October 12, 2020, from https://www.spiedigitallibrary.org/conference-proceedings-of-spie/2134/0000/*Ultraviolet-eye-damage-the-epidemiological-evidence/10.1117/12.180812.short?SSO=1*

Ultraviolet radiation: DNA damage, repair, and human disorders | SpringerLink. Retrieved October 12, 2020, from https://link.springer.com/article/10.1007/s13273-017-0002-0

Veronovski, N., Lešnik, M., & Verhovšek, D. (2014). *Surface treatment optimization of pigmentary TiO2 from an industrial aspect. Journal of Coatings Technology and Research, 11*(2), 255–264.

Vinod, P. N., & Lal, M. (2005). *Surface and optical characterization of the porous silicon textured surface for application in photovoltaics. Conference Record of the Thirty-First IEEE Photovoltaic Specialists Conference, 2005., 1135–1138.* https://doi.org/10.1109/PVSC.2005.1488336

Wang, H. W., Tsai, M. A., Chen, H. C., Tsai, Y. L., Tseng, P. C., Jang, C. Y., Yu, P., & Kuo, H. C. (2010). *Efficiency enhancement InGaP/GaAs dual-junction solar cell with sub-wavelength antireflection nanorod arrays. 2010 35th IEEE Photovoltaic Specialists Conference, 002132–002134.* https://doi.org/10.1109/PVSC.2010.5615959

Wang, K. X., Yu, Z., Sandhu, S., Liu, V., & Fan, S. (2014). *Condition for perfect antireflection by optical resonance at material interface. Optica, 1*(6), 388–395.

Wang, R. H., Xin, J. H., & Tao, X. M. (2005). *UV-blocking property of dumbbell-shaped ZnO crystallites on cotton fabrics. Inorganic Chemistry, 44*(11), 3926–3930.

Wang, Y., Chen, L., Yang, H., Guo, Q., Zhou, W., & Tao, M. (2009). *Spherical antireflection coatings by large-area convective assembly of monolayer silica microspheres. Solar Energy Materials and Solar Cells, 93*(1), 85–91. https://doi.org/10.1016/j.solmat.2008.08.008

Yamaguchi, S. (1962). *Theory of the Optical Properties of Very Thin Inhomogeneous Films. Journal of the Physical Society of Japan, 17*(1), 184–193. https://doi.org/10.1143/JPSJ.17.184

Yang, W., Wang, X., Gogoi, P., Bian, H., & Dai, H. (2019). *Highly transparent and thermally stable cellulose nanofibril films functionalized with colored metal ions for ultraviolet blocking activities. Carbohydrate Polymers, 213,* 10–16. https://doi.org/10.1016/j.carbpol.2019.02.085

Yerokhov, V. Y., & Melnyk, I. I. (1999). *Porous silicon in solar cell structures: A review of achievements and modern directions of further use. Renewable and Sustainable Energy Reviews, 3*(4), 291–322. https://doi.org/10.1016/S1364-0321(99)00005-2

Zeman, E. J., & Schatz, G. C. (1987). *An accurate electromagnetic theory study of surface enhancement factors for silver, gold, copper, lithium, sodium, aluminum, gallium, indium, zinc, and cadmium. Journal of Physical Chemistry, 91*(3), 634–643.

Zhang, H., & Zhu, H. (2012). *Preparation of Fe-doped TiO2 nanoparticles immobilized on polyamide fabric. Applied Surface Science, 258*(24), 10034–10041.

Zhang, Y., Blewett, T. A., Val, A. L., & Goss, G. G. (2018). *UV-induced toxicity of cerium oxide nanoparticles (CeO 2 NPs) and the protective properties of natural organic matter (NOM) from the Rio Negro Amazon River. Environmental Science: Nano, 5*(2), 476–486.

Zhao, X., Zhang, F., Xu, S., Evans, D. G., & Duan, X. (2010). *From layered double hydroxides to ZnO-based mixed metal oxides by thermal decomposition:*

Transformation mechanism and UV-blocking properties of the product. Chemistry of Materials, *22*(13), 3933–3942.

Zheng, B., Wang, Z., Guo, Q., & Zhou, S. (2016). *Glass composite as robust UV absorber for biological protection. Optical Materials Express*, *6*(2), 531–539.

APPENDIX-I

Polarization of a point charge:

Consider a positive point charge *q* placed at the origin of an infinite dielectric medium of electric permittivity ε'. We need to find polarization and polarization charges. Since the system has a spherical symmetry, we can use a Gauss's law to find the electric displacement D:

$$\oint_s D.\mathrm{nda} = \mathrm{q},$$

where the integration is performed over a sphere of radius *r* centered at the origin. This leads to

$$D = \frac{q}{4\pi r^2}\hat{r},$$

Consequently the electric field is

$$E = \frac{D}{\varepsilon'} = \frac{q}{4\pi\varepsilon' r^2}\hat{r}$$

Now, the polarization is

$$P = D - \varepsilon_0 E = \frac{q}{4\pi r^2}\hat{r} - \frac{\varepsilon_0 q}{4\pi\varepsilon' r^2}\hat{r} = \frac{q}{4\pi}\left(1 - \frac{\varepsilon_0}{\varepsilon'}\right)\frac{\hat{r}}{r^2} = \frac{q}{4\pi\varepsilon'}\left(\varepsilon' - \varepsilon_0\right)\frac{\hat{r}}{r^2}$$

$$P = \frac{q}{4\pi\varepsilon'}\left(\varepsilon - 1\right)\frac{\hat{r}}{r^2}$$

Where, macroscopic relative permittivity $\varepsilon \to \varepsilon'/\varepsilon_0$

Hence $P = \frac{(\varepsilon - 1)}{4\pi}E$

For a certain volume V of the material with polarization P the total dipole moment is given by

$$d_{tot} = VP = V\frac{(\varepsilon - 1)}{4\pi}E$$

APPENDIX-II

Alternate T-Matrix Method:

If we use matrix method, the characteristic matrix of a single film on a substrate is given by

$$\begin{bmatrix} E_I \\ H_I \end{bmatrix} = \begin{bmatrix} \cos\delta_1 & \dfrac{i\sin\delta_1}{n_1} \\ in_1\sin\delta_1 & \cos\delta_1 \end{bmatrix} \begin{bmatrix} E_{II} \\ H_{II} \end{bmatrix}$$

$$\begin{bmatrix} E_I / E_{II} \\ H_I / E_{II} \end{bmatrix} = \begin{bmatrix} B \\ C \end{bmatrix} = \begin{bmatrix} \cos\delta_1 & \dfrac{in_m\sin\delta_1}{n_1} \\ in_1\sin\delta_1 & n_m\cos\delta_1 \end{bmatrix} \begin{bmatrix} 1 \\ H_{II} / E_{II} \end{bmatrix}$$

$$\begin{bmatrix} B \\ C \end{bmatrix} = \begin{bmatrix} \cos\delta_1 & \dfrac{i\sin\delta_1}{n_1} \\ in_1\sin\delta_1 & \cos\delta_1 \end{bmatrix} \begin{bmatrix} 1 \\ n_m \end{bmatrix}$$

$$\begin{bmatrix} B \\ C \end{bmatrix} = \begin{bmatrix} \cos\delta_1 & \dfrac{in_m\sin\delta_1}{n_1} \\ in_1\sin\delta_1 & n_m\cos\delta_1 \end{bmatrix}$$

$$B = \cos\delta_1 + \frac{in_m\sin\delta_1}{n_1}$$

$$C = n_m\cos\delta_1 + in_1\sin\delta_1$$

For double layer

$$\begin{bmatrix} B \\ C \end{bmatrix} = \begin{bmatrix} \cos\delta_1 & \dfrac{i\sin\delta_1}{n_1} \\ in_1\sin\delta_1 & \cos\delta_1 \end{bmatrix} \begin{bmatrix} \cos\delta_2 & \dfrac{i\sin\delta_2}{n_2} \\ in_2\sin\delta_2 & \cos\delta_2 \end{bmatrix} \begin{bmatrix} 1 \\ n_3 \end{bmatrix}$$

The amplitude reflection coefficient is

$$r = \frac{n_o' - C/B}{n_o' + C/B}$$

Where $n_o^{'} = n_o \cos\theta$

Hence, reflectance $R=r^2$

BIODATA

SUNIL DEKA

House no. 5 , Amarpath, Dakshingaon Tiniali
Kahilipara, Guwahati, Assam, India -781019

+91-9613590056

dekasunil@rediffmail.com
sunil.deka@dbuniversity.ac.in

Work experience

2011- Today	Don Bosco University Assistant Professor Teaching Subject: Power Electronics, Control System, Energy Audit and management
2009-2011	Power Grid Corporation of India Limited Assistant Engineer Instillation and commissioning of bay extension in Substation, transmission of high tension power line and distribution of low tension line
2007-2008	Cognizant Technology Solution private India Limited Programmer Analyst Datawarehousing using ETL – Informatica, Business objects

Education

2012- 2014	Don Bosco University Master in Technology (76.6%) Department of Electronics and Communication Specialized in Opto-electronics and optical communication
2003-2007	Sathyabama University (85.4 %) Bachelor in Engineering Department of Electrical and Electronics

Additional Skills and achievement

Language:	Assamese, Hindi, Bengali and English
Software Language:	C++, Computational Electromagnetics – Transfer Matrix Method, Scattering Matrix method, Finite difference time domain.
Achievement:	First class with Distinction in Bachelor in Engineering, Organizing secretary of International conference ICERME-2021.